LAWRENCE
LIVERMORE
NATIONAL
LABORATORY

LLNL-JRNL-793010

Irrigation Impact on Water and Energy Cycle During Dry Years over the United States using Convection-permitting WRF and a Dynamical Recycling Model

Z. Yang, Y. Qian, Y. Liu, L. K. Berg, H. Hu, F. Dominguez, B. Yang, Z. Feng, W. I. Gustafson, M. Huang, Q. Tang

October 8, 2019

Journal of Geophysical Research: Atmospheres

Disclaimer

This document was prepared as an account of work sponsored by an agency of the United States government. Neither the United States government nor Lawrence Livermore National Security, LLC, nor any of their employees makes any warranty, expressed or implied, or assumes any legal liability or responsibility for the accuracy, completeness, or usefulness of any information, apparatus, product, or process disclosed, or represents that its use would not infringe privately owned rights. Reference herein to any specific commercial product, process, or service by trade name, trademark, manufacturer, or otherwise does not necessarily constitute or imply its endorsement, recommendation, or favoring by the United States government or Lawrence Livermore National Security, LLC. The views and opinions of authors expressed herein do not necessarily state or reflect those of the United States government or Lawrence Livermore National Security, LLC, and shall not be used for advertising or product endorsement purposes.

Irrigation Impact on Water and Energy Cycle During Dry Years over the United States using Convection-permitting WRF and a Dynamical Recycling Model

Zhao Yang[1*], Yun Qian[1*], Ying Liu[1], Larry K. Berg[1], Huancui Hu[1], Francina Dominguez[2], Ben Yang[3], Zhe Feng[1], William I. Gustafson Jr.[1], Maoyi Huang[1] and Qi Tang[4]

1. Pacific Northwest National Laboratory
2. Department of Atmospheric Sciences, University of Illinois, Urbana-Champaign
3. School of Atmospheric Sciences, Nanjing University, China
4. Lawrence Livermore National Laboratory

**Corresponding authors:*

Zhao Yang zhao.yang@pnnl.gov

Yun Qian yun.qian@pnnl.gov

Key Points:

- Irrigation increases evapotranspiration and the associated latent heat flux, cools surface air temperature and reduces sensible heat flux.
- Irrigation leads to enhanced moisture flux divergence over the irrigated regions.
- Irrigation intensifies the hydrologic cycle, highlighted by increased precipitation, evapotranspiration, and recycling ratio.

Abstract

An irrigation scheme is implemented in the Weather Research and Forecasting (WRF) model to investigate irrigation impacts over the Continental US (CONUS). Four major irrigated regions and two downwind regions were chosen to understand irrigation impacts over different climate regimes with a focus on irrigation-induced changes on the water and energy cycles. The Dynamic Recycling Model (DRM) is employed to quantify precipitation induced by irrigation and the precipitation recycling ratios over each irrigated region. With the irrigation scheme, WRF improves the simulated precipitation, surface skin temperature, and energy fluxes compared to reference datasets. For the energy cycle, irrigation increases latent heat flux over the irrigated regions along with reduced sensible heat flux. The evaporative cooling effect induced by irrigation leads to a cooler surface and less outgoing longwave radiation at the surface. Irrigation also intensifies the hydrological cycle over the irrigated regions, reflected by the increased precipitation, evapotranspiration, recycling ratio, and moisture export. Downwind regions exhibit increased precipitation and evaporation, decreased moisture flux divergence, and less consistent variations in recycling ratio. The precipitation increases over the irrigated regions can be partly explained by the more unstable low-level conditions, while reduced net moisture export is coincident with the precipitation increases over the downwind regions.

1 Introduction

Irrigation, by adding extra water into the soil, can modify energy partitioning between sensible and latent heat flux and consequently leads to a cooling effect on daytime temperature, which has been shown by both observational and modeling studies (e.g. Adegoke et al. 2003; Mahmood et al. 2006; Sacks et al. 2009). Numerous studies have demonstrated irrigation cooling effect on daytime temperature from regional to global scales (Ozdogan et al. 2010; Qian et al. 2013; Huang and Ullrich 2016; Yang et al. 2016; Yang et al. 2017; Sacks et al. 2008). However, irrigation effects on nighttime temperature still remains unclear and contrasting results have been reported (e.g., Bonfils and Lobell 2007; Kanamaru and Kanamitsu 2008).

Irrigation's effect on precipitation is more uncertain and complex, partly due to a number of positive and negative feedbacks occurring at the land and atmosphere interface. From the local perspective, irrigation cools the surface temperature and increases the surface moisture, which have opposing effects on the development of convective precipitation over the irrigated areas. Increasing low level moisture from irrigation leads to more convective available potential energy (CAPE), which is conducive to producing more convective precipitation (Crook 1996; Pielke 2001; Yang et al. 2017). In contrast, cooler surface temperature increases convective inhibition (CIN; Bluestein 1993), which makes it more difficult to initiate convection (Crook 1996; Boucher et al. 2004; Sacks et al. 2009; DeAngelis et al. 2010). From the non-local perspective, irrigation can influence regional precipitation by transporting water vapor downwind (Yang et al. 2017; Lo and Famiglietti 2013; DeAngelis et al. 2010) and through irrigation-induced secondary atmospheric circulations (Kanamitsu and Mo 2003; Yang et al. 2017). Irrigation can also lead to changes in soil moisture memory, which could induce seasonal precipitation changes (Koster and Suarez 2001; Rene and Seneviratne 2012). When combined, all of these factors results in a complex response of regional precipitation to irrigation.

Previous studies investigating irrigation impact have either focused on an intensely irrigated region, such as the California Central Valley, the Great Plains in the United States, or the Niger River in the West Africa, using regional climate models (RCM; e.g., DeAngelis et al. 2010; Qian et al. 2013; Marcella and Eltahir, 2013; Huber et al. 2014; Yang et al. 2016; Huang and Ullrich, 2016; Yang et al. 2017, among others) or global scale irrigation with global climate models (GCM; e.g., Boucher et al. 2004; Sacks et al. 2008; Puma and Cook 2010), while research on the impact of irrigation on the continental scale is still lacking (e.g., Ozdogan et al. 2010; Saeed et al. 2013; Pei et al. 2016). In addition, large uncertainties associated with convective parameterizations lead to large uncertainties in the location, intensity and amount of convective precipitation (e.g., Yang et al. 2012; Hohenegger et al. 2009), which subsequently influence the soil moisture and land atmosphere interactions (e.g., Hohenegger et al. 2009; Taylor et al. 2013). This study intends to bridge the gap between the regional and global scale irrigation studies by quantifying the irrigation impact on the continental scale with convection-permitting resolution for better simulation of precipitation processes. The objectives of this study are two-fold:

a) *Understanding irrigation impact on the surface and atmospheric water and energy budgets*. The water and energy analyses are performed to understand the irrigation impact on the water and energy budgets across different climate regimes. These analyses serve as a basis for understanding the irrigation impact on precipitation over and downwind of the irrigated regions. Due to the large variability of climatology over the US, four major irrigated regions, including the California Central Valley (CCV), Columbia River Basin (CRB), the Great Plains

(GPs) and the Mississippi River Valley (MRV), as well as two major downwind regions, i.e., the Midwest (MW) and the Southeast (SE) are chosen to perform the analysis (see Figure 1).

b) *Understanding irrigation impact on precipitation from the irrigated regions*. A back-trajectory technique (i.e., Dynamic Recycling Model: DRM) based on Dominguez et al. 2006 is employed to understand where evapotranspiration from the irrigated regions falls as precipitation over the domain. Earlier attempts by DeAngelis et al. (2010) and Harding and Snyder (2012) have employed the same model to investigate the irrigation impact of the Great Plains. To the best of the authors' knowledge, no previous studies have demonstrated the irrigation impact on the continental scale using the DRM.

This paper is organized as follows, Section 2 introduces the methodology, including a brief description of the irrigation scheme and the DRM model. Section 3 presents the validation of the model performance and results. Section 4 presents the conclusion and discussion.

2 Methodology

2.1 Model setup

To evaluate the impact of irrigation on the surface and atmospheric water budget, radiation budget, and moisture flux over the CONUS, two simulations were performed using the Advanced implementation of the Weather Research and Forecast Model (WRF) version 3.8.1 (Skamarock et al. 2008): one with the irrigation scheme (hereafter, IRRG; described in section 2.3) and one without the irrigation scheme (hereafter, CNTL). The model domain encompasses the entire CONUS with its spatial extent shown in Figure 1. To better resolve convective processes, we use 4 km horizontal grid spacing with convective parameterization turned off. There are 64 vertical levels with top of the atmosphere pressure at 50 hPa. Physical parameterizations used in the model include: Thompson microphysics (Thompson et al. 2008), RRTMG radiation (Iacono et al. 2008), MYNN planetary boundary layer physics (Nakanishi and Niino, 2006) and Noah land surface model (LSM; Chen et al. 1996). Wind, temperature, water vapor, pressure, and underlying surface variables including soil moisture and surface temperature that are used to generate initial and boundary conditions are derived from the NCEP FNL (Final) Operational Global Analysis data that are provided on 1-degree grid resolution at every six hours (NCEP, 2000). Continuous simulations were performed to represent two separate years starting from March 15 through October 31 in 2011 and 2012, respectively. No nudging is employed to the simulations. 2011 ranks as the third driest year in terms of annual precipitation and 5th driest in terms of JJA precipitation from 1981 to 2014 over the Great Plains based on the PRISM precipitation (Daly et al. 2008). In 2012, drought conditions were prevalent in many heavily irrigated regions, including the most severe drought in the Central Great Plains since 1895 (Hoerling et al. 2014). The reason for choosing two dry years is that irrigation is expected to have less impact on regional climate during wet years (Qian et al. 2013). Two dry years were included to add robustness to the analysis while fitting with available computational resources.

2.2 Reference Datasets

a. Precipitation datasets

Four precipitation reference datasets are chosen to minimize the uncertainty that may result from the application of a single product. The precipitation reference datasets employed in this study include:

i) Parameter-elevation Relationships on Independent Slopes Model (PRISM)

PRISM precipitation data is the official spatial climate dataset of the U.S. Department of Agriculture. It is available at 4 km resolution at daily time scale. PRISM calculates a climate-elevation regression for each digital elevation model grid cell and considers different factors of the terrain that may influence the precipitation, including location, elevation, coastal proximity, topographic facet orientation, vertical atmospheric layer, topographic position, and orographic effectiveness of the terrain (Daly et al. 2008). Data is available online at http://prism.oregonstate.edu/.

ii) NCEP Stage IV precipitation

The Stage IV precipitation product is a near-real-time product that is based on the NEXRAD precipitation processing system (Fulton et al. 1998) and the NWS River Forecast Center precipitation (RFC) processing (Seo and Breidenbach 2002). Stage IV data are mosaicked data from the 12 RFCs. Precipitation data from each RFC is sent to NCEP, which compiles the mosaic and provides the gridded precipitation estimates at 4 km with 1-hourly and 6-hourly intervals (Nelson et al. 2016). Nelson et al. (2016) evaluated the Stage IV precipitation estimates and showed their usefulness, in particular for medium to heavy precipitation, although the Stage IV suffers discontinuity problems due to data merging and different processing algorithms used at different RFCs. Data is available at http://www.emc.ncep.noaa.gov/mmb/ylin/pcpanl/stage4/.

iii) NSSL Multi-Radar/Multi-Sensor (MRMS)

The MRMS system was initially developed at the National Severe Storms Laboratory (NSSL) and the University of Oklahoma (Zhang et al. 2016). It integrates input from about 180 operational radars into a radar base map with very high spatial (1 km) and temporal (2 min) resolution. Then the radar base map is integrated with atmospheric environmental data along with other observation data, including satellite data, lightning and rain gauge observations to provide quantitative precipitation estimation products. The MRMS precipitation data used in this study employs a rain gauge bias correction to the radar precipitation estimates at 1 km spatial and hourly temporal resolution. Data is available at: https://www.nssl.noaa.gov/projects/mrms/.

iv) TRMM

The Tropical Rainfall Measuring Mission (TRMM) is a joint mission between NASA and the Japan Aerospace Exploration Agency (JAXA) designed to monitor and study tropical rainfall (Huffman et al. 2007). The 3B42 algorithm produces rain gauge adjusted multi-satellite precipitation rate and root-mean-square precipitation-error estimates. TRMM 3B42 dataset provides 3-hourly precipitation datasets with 0.25° spatial resolution spanning 50°S to 50°N from March 2000. Data is available at https://pmm.nasa.gov/data-access/downloads/trmm.

b. Surface meteorology and flux measurements

Observational sites over the Southern Great Plains that measure surface variables including

precipitation, air temperature and surface energy fluxes are shown in Figure 1. These networks include: Department of Energy Atmospheric Research Measurement (ARM) User Facility Surface Meteorology Systems (MET), The Oklahoma Mesonet stations (OKM, number of stations: 127), and Kansas Mesonet (KAM, number of stations: 13). These networks use conventional in situ sensors to obtain surface meteorological variables such as surface wind speed, wind direction, air temperature, relative humidity, barometric pressure, and precipitation.

Surface energy fluxes are available at the ARM sites. The ARM network measures surface latent (LH) and sensible heat fluxes (SH) at the eddy correlation (ECOR) and energy balance Bowen ratio (EBBR) stations (http://www.arm.gov/instruments/ecor; http://www.arm.gov /instruments/ebbr). The EBBR calculates bulk aerodynamic LH and SH for periods when the Bowen ratio is between -1.6 and -0.45 (to reduce uncertainties near sunset and sunrise). ARM has enhanced the ECOR systems through series of quality control procedures, and this study employs the best estimate of the ARM station-based surface datasets (Tang and Xie 2015, Tang et al. 2018).

2.3 Irrigation scheme

The irrigation scheme is added to the Noah LSM to account for the anthropogenic water source. It is implemented in a similar way as the irrigation scheme used in Qian et al. 2013. The Noah LSM has four layers with depth of 0.1, 0.3, 0.6 and 1.0 m, extending from the surface to 2 m under ground. The Noah LSM has a free drainage at the bottom layer without accounting for the exchange of water flux between the free water table and soil column (Martinez et al. 2016). Irrigation is applied only to grassland and cropland, based on the Moderate Resolution Imaging Spectroradiometer (MODIS) 20-category land use and land cover dataset.

The key questions that an irrigation scheme need to address are: a) where to irrigate, b) when to irrigate and c) how much to irrigate.

a) Where to irrigate

An irrigation fraction map is used to indicate where irrigation might occur. In this study it is obtained from the Food and Agriculture Organization of the United Nations (Siebert et al. 2013). Irrigation is only applied to grid cells identified as grassland or cropland with irrigation fraction greater than 0.

b) When to irrigate

Irrigation is triggered during the growing season which is defined based on a threshold using greenness vegetation fraction (GVF), see (1) below.

$$\mathrm{GVF}_{\mathrm{thresh}} = \mathrm{GVF}_{\mathrm{min}} + 0.4 \times (\mathrm{GVF}_{\mathrm{max}} - \mathrm{GVF}_{\mathrm{min}}), \tag{1}$$

where GVFmax and GVFmin represent the climatological annual maximum and minimum GVF, respectively. During growing season, irrigation is activated when moisture availability (MA, defined in (2)) is below a specified threshold.

$$\mathrm{MA} = \frac{\mathrm{SM} - \mathrm{SM}_{\mathrm{WP}}}{\mathrm{SM}_{\mathrm{FC}} - \mathrm{SM}_{\mathrm{WP}}}, \tag{2}$$

where SM is the current soil moisture, $\mathrm{SM}_{\mathrm{WP}}$ and $\mathrm{SM}_{\mathrm{FC}}$ denote the soil field capacity and wilting point, respectively.

c) How much to irrigate

Once irrigation is triggered, the amount of water applied is the difference between the current soil moisture content and field capacity of the root zone. Irrigated water will be added as precipitation evenly from 6 a.m. to 10 a.m. local time to mimic typical overhead sprinkler operation. More details for the irrigation scheme can be found in Qian et al. (2013) or Ozdogan et al. (2010).

The amount of water irrigated over grid boxes with irrigation fraction greater than 0.1 is shown in Figure 2. A clear seasonal pattern is shown with intense irrigation during the JJA growing season. The most intense irrigation occurs in July and then gradually diminishes until the end of the simulation. According to Sorooshian et al. (2011) and Hanson et al. (1999), the long-term average amount of irrigation applied over the CCV is around 350 mm year^{-1}. Here, our simulation tends to overestimate irrigation amount with 486 (539) mm year^{-1} for 2011 (2012) over the same region. Since both 2011 and 2012 are drought years (Wei et al. 2016), overestimating the average irrigation is expected. The objective of this study is to investigate the impact induced by incorporating irrigation into the model. Bearing that in mind, caution should be warranted when interpreting the results and extrapolating beyond the simulated years.

2.4 Surface and atmospheric moisture budget analysis

To evaluate changes induced by irrigation on the surface, each component in the surface water budget is represented in equation (3) (all in mm/day):

$$dSM = P - ET - udroff - sfroff + IRR \tag{3}$$

where *dSM* is the change in soil moisture content, *P* is precipitation, *ET* is evapotranspiration, *udroff* and *sfroff* are runoff generated under the ground and on the surface, and *IRR* is the irrigation amount, if any. Irrigation induced changes in each component in (3) are presented for the four irrigated and two downwind regions shown in Figure 1, to show the distinct impact of irrigation at different climate regimes across the US.

Changes in atmospheric moisture content is determined through local evapotranspiration and moisture flux convergence, which are connected to soil moisture via boundary layer processes and atmospheric circulations (Kanamitsu and Mo 2003). In other words, regional precipitation on a seasonal timescale is roughly a balance between local change in atmospheric moisture storage, local evaporation, and remote moisture transport (Brubaker et al. 1993). It can be formulated as:

$$\frac{1}{g}\frac{\partial}{\partial t}\int_{Pt}^{Ps} q\,dp = ET - P - \frac{1}{g}\nabla\cdot\int_{Pt}^{Ps} V\cdot q\,dp \tag{4}$$

where $dPW = \frac{1}{g}\frac{\partial}{\partial t}\int_{Pt}^{Ps} q\,dp$ is the change in atmospheric moisture storage, ET is evaporation, P is precipitation, q is specific humidity, V is the horizontal wind, P_t is the pressure at the top of the atmosphere, P_s is the surface pressure, $\frac{1}{g}\nabla\cdot\int_{Pt}^{Ps} V\cdot q\,dp$ is the moisture flux divergence (MFD) which represents the net moisture transported into and out of an atmospheric column. MFD is

further decomposed into horizontal moisture advection (HA) and horizontal velocity divergence (HD) following (5),

$$MFD = \frac{1}{g}\int_{Pt}^{Ps} V \cdot \nabla q dp + \frac{1}{g}\int_{Pt}^{Ps} q \cdot \nabla V dp \tag{5}$$

where HA and HD are the first and second terms on the right side of equation (5), respectively. Similar to the surface water budget, for each term only changes induced by irrigation are shown to indicate the irrigation impact (all in mm/day).

2.5 Moisture tracking using the DRM

To separate the influence of irrigation over the irrigated regions delineated in Figure 1, we perform a detailed investigation of the evaporative source of precipitation using the DRM (Dominguez et al. 2006; Martinez and Dominguez, 2014). The DRM is a 2D analytical model that accounts for moisture storage and assumes a well-mixed atmosphere. Compared to other simpler analytical models that do not include the moisture storage term (Brubaker et al. 1993; Eltahir and Bras, 1996), the DRM can be used at daily time scales (Dominguez et al. 2006). The well-mixed assumption implies that the ratio of local recycled precipitation is equal to the ratio of local evapotranspiration to total precipitable water in the atmospheric column. Combining the mass conservation for both advected and local moisture, the fraction of atmospheric moisture collected by an air column along its trajectory is formulated as follows after introducing a Lagrangian coordinate system with $\chi = x - ut$, $\xi = y - vt$, and $\tau = t$.

$$R(\chi,\xi,\tau) = 1 - \exp[-\int_0^{\tau} \frac{\varepsilon(\chi,\xi,\tau)}{\omega(\chi,\xi,\tau)} \partial\tau'] \tag{6}$$

where $\varepsilon(\chi,\xi,\tau)$ is the evapotranspiration, $\omega(\chi,\xi,\tau)$ is the precipitable water along the two-dimensional trajectory (χ,ξ). Martinez and Dominguez (2014) extended the DRM to quantify the relative contributions from different sources to the atmospheric moisture over a given sink region. In this study, the extended DRM is used to determine the distribution of irrigation-induced precipitation from each of the irrigated regions. There are two options to evaluate the irrigation-induced precipitation, one is to define the source region as the irrigated grid cells only, and the other is to define the source region as the irrigated cells along with their surrounding non-irrigated grid cells. We argue that because this back-trajectory technique links precipitation over one grid cell to ET in the upstream grid cells and irrigation changes ET both in the irrigated grid cells and their nearby non-irrigated grid cells, that it would be more informative to include both cell types when evaluating the irrigation induced precipitation.

The DRM is run for both the CNTL and IRRG simulations to obtain the fraction of precipitation from a given source region. The amount of precipitation from the source region ET is then multiplied by the fraction with total precipitation to yield a weighted contribution. Finally, the irrigation-induced precipitation is calculated as the difference between the CNTL and the IRRG simulation.

3 Results:

3.1 Model evaluation of precipitation, surface fluxes and surface skin temperature

To estimate the impact of irrigation on regional climate, it is imperative that the WRF model is able to realistically represent the surface variables such as precipitation, surface energy fluxes, and surface temperature. Here precipitation is evaluated against four reference datasets to minimize the uncertainties that may be associated with a single product. The comparison is performed for 2012 (conclusion remains the same for 2011 and not shown). An overall west-east gradient in precipitation is observed from the precipitation spatial pattern with wetter conditions towards the east (Figure 3). Daily precipitation with more than 3 mm day^{-1} occurred over the southeast coast of the US while dry conditions are shown in the Southwest with almost no precipitation occurred over California. Different reference datasets are in good agreement both in terms of spatial pattern and magnitude. Slight differences do exist, for example, TRMM shows larger precipitation over the central Great Plains and Midwest than other reference datasets. Compared to the references, the CNTL simulation clearly underestimates precipitation over the central and Southeast US, including the Great Plains and southeast coastal areas. Adding irrigation reduces the bias in the CNTL simulation, indicated by the reduction in absolute bias in Figure 3i, leading to more consistent spatial pattern with the four reference datasets. Heavy precipitation associated with mesoscale convective systems is also largely improved in the IRRG simulation both in terms of location and timing (not shown).

To further assess the capability of the irrigation scheme, surface variables extracted from the SGP observation sites shown in Figure 1 are compared against the simulated variables over grid boxes where observations are available (see Figure 4). The warm and dry biases in the CNTL simulation are both reduced by application of the irrigation scheme. Warm bias in temperature is reduced from 1.9 to 0.7 K while the dry bias is reduced from 24.0 to 19.4 mm month^{-1}. Simulated LH and SH also tends to be closer to the SGP observations in both years in the IRRG simulation. Biases in LH and SH are reduced from 18.7 and 22.0 W m^{-2} to 10.3 and 20.2 W m^{-2}, respectively. Overall, irrigation reduces model bias in the simulated precipitation, surface temperature, and energy fluxes, indicating that it is important to include irrigation in modeling the land surface processes.

3.2 Irrigation Effects on Surface Water and Energy Balance

Since irrigation adds additional water to the land surface, it directly changes the surface energy budget and water balance. The response of surface variables to irrigation is shown in this section. The results of the IRRG run are compared with the CNTL run and the difference of the two simulations show the irrigation impact. We choose to focus on JJA because irrigation is most intense during these summer months (Figure 2).

In general, for the two JJA seasons the amount of irrigated water is dependent on the geographic location and climate regimes. In comparison with precipitation, the amount of water irrigated is almost comparable or even more than the precipitation amount over the irrigated regions in CCV, CRB, GPs and MRV. This also speaks to the necessity to include an irrigation scheme in the climate models.

Figure 5a and 5b show the JJA soil moisture (from the surface to a depth of 10 cm) change due to irrigation. Overall, the additional water input by irrigation increases soil moisture primarily over the irrigated regions. Outside the irrigated regions, the SE and MW generally show an increase in soil moisture as well, especially later in the summer (not shown), likely to be associated with changes in precipitation. Compared to precipitation, irrigation water and ET show more

localized changes over the irrigated area, whereas changes in precipitation are most obvious over the MW and east US in the downwind regions (Figure 5 c-h).

Changes in soil moisture for different soil layers indicate that irrigation generally increases soil moisture in the top meter (not shown). This is related to how irrigation is prescribed. Since irrigation here is specified as sprinkler-type, which behaves in a similar way as precipitation (Qian et al. 2013). As a result, the majority of the added water evaporates to the atmosphere or becomes surface runoff before the water infiltrates deeper into the soil column.

Figure 6 shows the changes in each component of the surface water budget (equation (1)) due to irrigation. An interesting feature is shown with transition from the west to the east. In the west, irrigation water shows the largest change in the budget and followed by evapotranspiration and, to a lesser extent, soil moisture storage. Further to the east in the downwind MW and SE, precipitation shows the largest increase, suggesting the non-local effect of irrigation on precipitation over non-irrigated regions. This also indicates that irrigation leads to more precipitation over the relatively wet eastern US, increasing the gradient of precipitation over the US by making the wet regions wetter.

Due to the additional water input, more available energy is partitioned into latent heat flux and less energy is available for the sensible heat flux (Figure 7). The evaporative cooling effect cools the surface skin temperature and reduces outgoing longwave radiation. The strongest irrigation impact is located over the GPs where irrigation is the largest of the regions included in this study. Over the GPs, latent and sensible heat fluxes are increased by 46.7 and -33.4 W m^{-2}, respectively, leading to an increase in net available energy by 13.2 W m^{-2} and a cooling of the surface skin temperature of ~2.5 K averaged over the two years. Analyzing the surface radiation budget reveals that the increase in available energy is directly related to the reduction in outgoing longwave radiation due to the decrease in surface skin temperature (Figure 7 and 8). For example, in the GPs changes in the incoming longwave and shortwave radiation are 2.4 and -1.0 W m^{-2}, respectively, whereas outgoing longwave radiation is decreased by 14.9 W m^{-2}. As a result, net radiation is increased by 13.3 W m^{-2}. In summary, irrigation increases surface evapotranspiration and the associated latent heat flux, reduces sensible heat flux and surface skin temperature due to the evaporative cooling effect. The reduced surface skin temperature emits less outgoing longwave radiation and in turn increases the surface available energy.

3.3 Irrigation effects on the atmospheric water budget

This section focuses on the variations in the atmospheric water budget in equation (2), which later serves as a basis for analyzing moisture sources and sinks in Section 3.4. Figure 9 shows the irrigation induced changes in precipitable water (PW), moisture flux divergence, and integrated water vapor flux (IWVF). When combined with changes in precipitation and evapotranspiration, a full description of the budget equation is described (see equation (4)). Overall, changes in the storage term are negligible when compared with other terms. There is coherent moisture flux divergence over the irrigated regions over the two years (Figure 9b, 9d), especially over the intensely irrigated GPs. IWVF shows northerly anomalies over the GPs in both years. The northerly anomaly is also seen in other studies investigating irrigation impacts over the GPs (e.g., Huber et al. 2014; Pei et al. 2016), suggesting a weakening of the Great Plains low-level jet. The weakening of the low-level jet will result in less moisture transport from the South (shown later).

The atmospheric water budget suggests that adding irrigation strengthens moisture flux divergence over the irrigated regions except for MRV in 2012 JJA (see Figure 10, increase in MFD indicates more moisture export). This suggests that adding irrigation generally increases the amount of moisture export from the irrigated region. On the contrary, the downwind MW and SE show decrease in MFD, meaning that moisture convergence or import is increased over the downwind regions in the IRRG simulations, consistent with additional export in these volumes from the irrigated areas.

Decomposition of MFD into HA and HD allows us to identify which process is responsible for the change in MFD. Note that negative HD indicates horizontal velocity convergence. In almost all regions, horizontal velocity convergence is strengthened in magnitude with the exception of CCV and 2012 MW. Previous studies have shown that mesoscale convergence can have a dominant role on cloud formation. Using a two-dimensional model, Chen and Orville (1980) showed that convergence can lead to strong convection. Leichter (1974) also found significant convection to be associated with mesoscale convergence. Given the convective nature of JJA precipitation, it suggests that precipitation increase is also associated with the enhanced horizontal velocity convergence. In contrast, HA is consistently increased over the irrigated CRB, GPs, and MRV, counteracting the effect of increased horizontal velocity convergence on MFD. In sum, changes in MFD is generally dominated by the increased HA, indicating that moisture export is mainly induced by horizontal moisture advection over these regions, likely because of the increased moisture gradient between the irrigated and non-irrigated regions. In contrast, the downwind regions MW and SE show decreased HA, meaning that both horizontal velocity convergence and horizontal moisture advection contribute to the reduction in MFD for these regions.

An interesting characteristic of the moisture budget is how the relative contributions changes when moving from the west to east across the country. The ET and MFD are the dominating factors over the west US (Figure 10). Over the central GPs and MW, P, ET, and MFD are of equal importance. Further to the east, P and ET are the dominating factors instead. This reflects the different behavior of the atmospheric moisture budget across different climate regimes over the US. This is seen both with and without irrigation, with the irrigation only adding a perturbation onto the dominant natural processes.

An examination of line integral of the vertically integrated moisture fluxes across each border of the boxes is shown in Figure 11. Zonal moisture fluxes are much stronger than the meridional components, with the exception of the GPs, where the meridional and zonal moisture transport are almost of equal magnitude. In the GPs low-level jets are responsible for transporting large amounts of moisture from the Gulf of Mexico (Berg et al. 2015). Over the GPs and MRV, irrigation has weakened the meridional moisture components while strengthening in the zonal component. This is likely associated with circulation changes and apparent weakening of the low-level jets associated with irrigation (see Figure 9). Even though moisture coming in from southern border into the GPs is less in the IRRG simulation, irrigation-induced ET partly compensates this loss of moisture and precipitation over the GPs is still increased (see Figure 6).

Note the sum of the moisture fluxes transported across four borders into a region (i.e., the net moisture fluxes in Figure 11) is equivalent to the regionally averaged negative MFD in Figure 10 (see derivation in Schmitz and Muller (1997) for details). Over irrigated regions, the amount of moisture export has been increased, as represented by the enhanced negative net moisture fluxes (Figure 11), consistent with the moisture flux divergence pattern seen in Figures 9b, 9d and Figure

10. Conversely, over the downwind regions, the amounts of moisture export are generally reduced except for 2012 MW. In the 2012 SE, there is even net import of moisture (sign reversed). The different behaviors of moisture export caused by irrigation over the irrigated and downwind regions have different implications on precipitation recycling (shown later).

3.4 Irrigation Effects on Moisture Transport

We have analyzed the irrigation induced changes in water and energy budget. However, how the water added over each irrigated region would affect precipitation across the US is still unknown. With DRM, this section aims to answer this important question.

The left column of Figure 12 shows the fraction of precipitation at each grid box that originates from ET in the source regions (indicated by the red boxes) for the CNTL simulations for 2012 JJA. Not surprisingly, ET influences the respective sources regions most strongly, as well as the nearby downwind regions. Overall, the CRB shows the highest fraction of precipitation (~0.15) over the northeastern side of the CRB. This indicates that the CRB ET tends to remain within the CRB compared to other regions. Over the GPs, precipitation fraction reaches values of ~0.12 locally over the northern Kansas and southern Nebraska and further affects its downwind regions including the Midwest. MRV ET mostly affects the southeastern US following the climatological wind direction.

This precipitation fraction multiplied by precipitation amount becomes the precipitation induced by source region ETs (see Figure 12 2nd column). The CCV ET induced precipitation shows more limited spatial extent and magnitude due to its dry climate. In contrast, the GPs and MRV ET contribute to much greater amount of precipitation. The difference in the amount of precipitation induced by source region ET between the IRRG and the CNTL is then the irrigation induced precipitation (shown in Figure 12 3rd column). The most intense irrigation induced precipitation is due to irrigation over the GPs, with differences up to 0.4 mm day^{-1} in Iowa, which amounts to an increase in precipitation of more than 20%. Compared to the GPs, other irrigated regions show less impact in terms of irrigation induced precipitation, although the spatial patterns of relative changes are more obvious (Figure 12 4th column). The relative change in precipitation induced by irrigation also suggests that the impact of irrigation could be far from its source region. For instance, irrigation over the CCV increases precipitation as far away as the northern GP, including areas in Nebraska, the Dakotas, and Minnesota, with increases up to ~8%; irrigation over the GP affects the central and eastern US with irrigation induced precipitation increases of more than 15%. The spatial extent of irrigation impacts on precipitation is much more far-reaching than previously reported.

Recycling ratio over each source region is also calculated. It is the fraction of precipitation coming from the local evapotranspiration to total precipitation over each box. In general, there is a consistent increase in recycling ratio over the irrigated regions. This increase is partly due to the increased ET, as well as the increase in moisture flux divergence (i.e., increased net moisture export, see Figure 10). As a result, local ET accounts for a larger fraction of precipitable water over the irrigated regions. Consequently, when it rains, the well-mixed assumption within the DRM yields a larger local recycling ratio over the irrigated regions. As an example, the recycling ratio over the GP increases from 0.063 to 0.11 for 2011 JJA and from 0.068 to 0.126 for 2012 JJA when irrigation is considered. The recycling ratio is more variable in the downwind regions. For example, the downwind SE region experiences a net gain of moisture due to horizontal moisture import in 2012 JJA (Figure 11). Even though local ET is increased, due to net import of moisture,

the recycling ratio is reduced from 0.105 (CNTL) to 0.097 (IRRG). Moisture is still exported out of the SE in 2011 and the recycling ratio is slightly increased from 0.068 to 0.078.

Irrigation induced precipitation, when averaged over irrigated regions, are 0.003, 0.03, 0.08 and 0.18 mm day^{-1} for the CCV, CRB, GP and MRV regions, respectively, while total precipitations increases are 0.02, 0.11, 0.29 and 0.42 mm day^{-1} over these irrigated regions according to our simulations. The difference between irrigation induced precipitation and total precipitation increase implies that moisture imported from external source also contributes to precipitation increase over irrigated regions. The consistent enhanced net moisture export over the irrigated regions implies that the efficiency of moisture to become precipitation should be higher. Figure 13 shows the vertical profile of moist static energy (MSE) over the GPs and SE for both daytime and nighttime. These two regions were selected to represent typical profiles over the irrigated and downwind regions. MSE is an indication of moist static instability and higher values are usually associated with more convective instability and higher probability to rain (Eltahir 1998). Over the GPs, there is larger MSE close to the ground in the IRRG simulations especially during the day, making it more unstable and easier to trigger precipitation. Over the downwind SE, MSE at low levels is slightly smaller in the IRRG simulations, indicating a more stable environment over the SE caused by irrigation. Therefore, precipitation increase over the SE is more related to moisture availability (less net moisture export), and less likely to be associated with changes in instability.

4 Discussion

It has been well established that due to the chaotic and non-linear nature of the atmospheric processes, global climate models are sensitive to initial conditions (Villarini and Vecchi 2012; Done et al., 2014). Regional climate models (RCM) have also shown to have internal variability, despite the fact that RCMs are forced by the lateral boundary conditions (Alexandru et al. 2007). The results of the RCM can be decomposed into two components: 1) a reproducible signal associated with the lower and boundary conditions and 2) an irreproducible component associated with internal variability (Giorgi and Bi 2000). Focusing on the internal variability of RegCM3 over South America, Kgatuke et al. 2007 indicated that the internal variability is small when seasonal totals are considered and there is strong reproducibility of the number of rain spells. Similarly, Yang et al. 2017 applied three ensemble members to investigate the irrigation impact over the California Central Valley. Irrigation-induced difference fields agree well and show consistent pattern among the ensemble members. Given the similarities in irrigation-induced differences in the two years simulated and that our results are focused on the JJA average, rather the day-to-day variability, we believe that the conclusions would not be significantly different if an ensemble were used, and we should draw the same conclusions even if more simulations are included.

The irrigation scheme employed in this study is rather simple and water-centric. We did not consider harvest time and the associated changes in surface conditions. Vegetation dynamic is treated following the default Noah LSM and represented by using the climatological GVF. We did not explicitly consider the different types of irrigation methods applied over the CONUS. While flood irrigation is also widely used in the US, here we only consider sprinkler-type irrigation because sprinkler irrigation is the dominate type (~51%) (Leng et al. 2017).

Our irrigation scheme tends to overestimate the amount of water applied based on rough comparisons to available irrigation water use from 2015 (not shown), which might be improved with further tuning of the irrigation scheme. Irrigated water amount is sensitive to the value of

MA, which is universally specified as 0.5 following Ozdogan et al. 2010. It would be extremely difficult to find an optimal value of MA to realistically represent irrigation amount across the entire US and that is beyond the scope of this study, particularly given the potential complexity that would be needed to make the simple scheme more robust. The conclusions drawn from this study are dependent on the experiment setup, simulation years, physical parameterizations and even the WRF model employed. Different model setup would be needed to address the modeling uncertainties in evaluating the irrigation impact on land atmosphere feedbacks. This could be done in a future study.

5 Conclusion

In this study, we have incorporated an irrigation scheme into the Noah land surface model coupled to the WRF model to represent anthropogenic impact of irrigation on regional climate. Specifically, we focus on irrigation induced changes in water and energy balance. Moreover, the impact of irrigation over each irrigated region is investigated using a moisture tracking DRM.

Our study shows that incorporating irrigation modifies surface water and energy balances. When compared against the reference datasets, the IRRG simulation outperform the CNTL simulation in terms of precipitation, surface temperature and energy fluxes. Irrigation has extensively modified the surface water and energy balance, both over and downwind of the irrigated regions. As intuitively expected, the surface water budget reveals that irrigation tends to increase evapotranspiration and soil moisture, especially over intense irrigation regions. Precipitation increases most over the downwind Midwest and the Southeast US regions in the irrigation simulations. With irrigation, there is also an overall increase in surface available energy, mainly induced by a reduction in outgoing longwave radiation caused by cooler surface skin temperatures. The partitioning of surface available energy shifts to having increased latent heat fluxes, which is compensated by reduced surface sensible heat fluxes.

Over the irrigated regions MFD is strengthened, predominately by changes in horizontal moisture advection. MFD is reduced downwind of irrigated regions, leading to a net gain of moisture in the IRRG as compared to CNTL simulations. Decomposition of MFD reveals that horizontal velocity convergence generally increases, consistent with changes in precipitation for all regions with the exception of the CCV.

The DRM is utilized to evaluate the irrigation impact from each irrigation region over the US. The GPs show the most obvious increase in irrigation induced precipitation with increased precipitation over the downwind regions to the northeast and east. Irrigation induced precipitation increases up to 20% occur in Iowa. A less intuitive result from this analysis is that the total simulated precipitation increase is greater than irrigation induced precipitation over each irrigated region. This is likely because over the irrigated region, a more unstable atmosphere contributes to the precipitation increase, as indicated by an increase in MSE at low levels over the irrigated regions. Since the recycling ratio is less than 1, there is always water vapor originating from outside the irrigated regions that contributes to precipitation. As such, total precipitation increase is a sum of contribution from within and outside the irrigated regions. Additionally, it is also possible that irrigation has altered atmospheric flow and therefore the import and export of moisture from the irrigated regions. Low-level jets of the Great Plains have been shown to be important for mesoscale convective systems (Feng et al. 2019). Future study will focus on irrigation impact on low-level jets. Over the downwind regions, the precipitation increase is more related to moisture amount, rather than changes in stability.

Figure 14 summarizes moisture fluxes across the borders, precipitation, evapotranspiration, and recycling ratio over each region. Overall, intensified hydrological cycle can be detected over the irrigated regions indicated by increased precipitation, evapotranspiration, as well as recycling ratio and increased net moisture export. The downwind regions feature increased precipitation, evapotranspiration, and decreased moisture export and variable changes in recycling ratio.

Through coupling an irrigation scheme to the land surface model in WRF and utilizing a DRM approach, this study has examined the water and energy balance and tracks ET that originates from each of the selected irrigated regions. We note that the DRM is a simple 2-dimensional analytical model that does not account for the vertical heterogeneity, which is important for precipitation related processes over some regions of the US (Hu and Dominguez 2015). However, based on comparisons with other models that calculated moisture contributions (e.g. Hoyos et al. 2017), we are confident that the DRM is able to capture the bulk tendencies in precipitation induced by irrigation. More accurate estimations accounting for vertical heterogeneity would require more sophisticated methods (e.g. water vapor "tagging" techniques in climate models) which can be explored in the future. The weakened Great Plains low level jet induced by irrigation, as reported in earlier studies, is also an interesting feature that is worth further investigation.

Acknowledge:

This research was supported by the Office of Science of the U.S. Department of Energy (DOE) as part of the Atmospheric System Research (ASR) Program via Grant KP1701000/57131. F. D. was supported by National Science Foundation (NSF) CAREER Award AGS 1454089. Q. T. was funded by Atmospheric Radiation Measurement program of the U.S. Department of Energy (DOE) under the auspices of the U.S. DOE by Lawrence Livermore National Laboratory under contract DE-AC52-07NA27344. The research used computational resources from National Energy Research Scientific Computing Center (NERSC), a U.S. DOE Office of Science User Facility operated under Contract DE-AC02-05CH11231. This work has benefited from discussion with Jerome Fast. Koichi Sakaguchi, and Heng Xiao. The Pacific Northwest National Laboratory is operated for DOE by Battelle Memorial Institute under Contract DE-A06-76RLO 1830. The authors declare no conflict of interests. Data and results are available at https://portal.nersc.gov/project/m1660/yang560/.

References:

Adegoke, J. O., R. A. Pielke, J. Eastman, R. Mahmood, and K. G. Hubbard (2003), Impact of irrigation on midsummer surface fluxes and temperature under dry synoptic conditions: A regional atmospheric model study of the U.S. high plains, *Monthly Weather Review*, *131*(3), 556–564, doi:10.1175/1520-0493(2003)131<0556:IOIOMS>2.0.CO;2.

Alexandru, A., R. de Elia, and R. Laprise (2007), Internal Variability in Regional Climate Downscaling at the Seasonal Scale, *Mon. Wea. Rev.,* 135, 3221–3238, https://doi.org/10.1175/MWR3456.1

Berg, L. K., L. D. Riihimaki, Y. Qian, H. Yan, and M. Huang (2015), The Low-Level Jet over the Southern Great Plains Determined from Observations and Reanalyses and Its Impact on Moisture Transport, *Journal of Climate*, *28*(17), 6682–6706, doi:10.1175/JCLI-D-14-00719.1.

Bi, X., F. Giorgi (2000), A study of internal variability of a regional climate model, *J. Geophys. Res.*, 105, 29503–29521.

Bluestein, H. B. (1993), Observations and Theory of Weather Systems. Vol. 2, Synoptic-Dynamic Meteorology in Midlatitudes, 594 pp Oxford University Press.

Bonfils, C., and D. Lobell (2007), Empirical evidence for a recent slowdown in irrigation-induced cooling, *Proc. Natl. Acad. Sci. U.S.A.*, *104*(34), 13582–13587, doi:10.1073/pnas.0700144104.

Boucher, O., G. Myhre, and A. Myhre (2004), Direct human influence of irrigation on atmospheric water vapour and climate, *Climate Dynamics*, *22*(6-7), 597–603, doi:10.1007/s00382-004-0402-4.

Brubaker, K. L., D. Entekhabi, and P. S. Eagleson (1993), Estimation of Continental Precipitation Recycling, *Journal of Climate*, *6*(6), 1077–1089, doi:10.1175/1520-0442(1993)006<1077:EOCPR>2.0.CO;2.

Chen, C.-H., and H. D. Orville (1979), Effects of Mesoscale Convergence on Cloud Convection, *Journal of Applied Meteorology*, *19*(3), 256–274, doi:10.1175/1520-0450(1980)019<0256:EOMCOC>2.0.CO;2.

Chen, F., K. Mitchell, J. Schaake, Y. Xue, H.-L. Pan, V. Koren, Q. Y. Duan, M. Ek, and A. Betts (1996), Modeling of land surface evaporation by four schemes and comparison with FIFE observations, *J. Geophys. Res.*, *101*(D3), 7251–7268, doi:10.1029/95JD02165.

Crook, N. A. (1996), Sensitivity of Moist Convection Forced by Boundary Layer Processes to Low-Level Thermodynamic Fields, *Monthly Weather Review*, *124*(8), 1767–1785, doi:10.1175/1520-0493(1996)124<1767:somcfb>2.0.co;2.

Daly, C., M. Halbleib, J. I. Smith, W. P. Gibson, M. K. Doggett, G. H. Taylor, J. Curtis, and P. P. Pasteris (2008), Physiographically sensitive mapping of climatological temperature and precipitation across the conterminous United States, *International Journal of Climatology*, *28*(15), 2031–2064, doi:10.1002/joc.1688.

DeAngelis, A., F. Dominguez, Y. Fan, A. Robock, M. D. Kustu, and D. Robinson (2010), Evidence of enhanced precipitation due to irrigation over the Great Plains of the United States, *J. Geophys. Res.*, *115*(D15), 959, doi:10.1029/2010JD013892.

Dee, D. P. et al. (2011), The ERA-Interim reanalysis: configuration and performance of the data assimilation system, *Quarterly Journal of the Royal Meteorological Society*, *137*(656), 553–597, doi:10.1002/qj.828.

Dominguez, F., P. Kumar, X.-Z. Liang, and M. Ting (2006), Impact of atmospheric moisture storage on precipitation recycling, *Journal of Climate*, *19*(8), 1513–1530, doi:10.1175/JCLI3691.1.

Done, J. M., C. L. Bruyère, M. Ge, and A. Jaye (2014), Internal variability of North Atlantic tropical cyclones, *Journal of Geophysical Research: Atmospheres*, 119(11), 6506–6519, doi:10.1002/2014JD021542.

Eltahir EAB, Bras RL (1996) Precipitation recycling. *Reviews of Geophysics* 34:367–378. doi: 10.1029/96RG01927

Eltahir, E. A. B. (1998), A Soil Moisture–Rainfall Feedback Mechanism: 1. Theory and observations, *Water Resour. Res.*, *34*(4), 765–776, doi:10.1029/97WR03499.

Feng, Z., R. A. Houze, R. Leung, F. Song, J. Hardin, J. Wang, W. I. Gustafson, C. R. Homeyer (2019), Spatiotemporal Characteristics and Large-scale Environments of Mesoscale Convective Systems East of the Rocky Mountains. J. Clim. Accepted.

Fulton, R. A., J. P. Breidenbach, D.-J. Seo, D. A. Miller, and T. O'Bannon (1998), The WSR-88D Rainfall Algorithm, *Wea. Forecasting*, *13*(2), 377–395, doi:10.1175/1520-0434(1998)013<0377:twra>2.0.co;2.

Hanson, B., L. J. Schwankl, A. Fulton, University of California Irrigation Program (1999), *Scheduling Irrigations: When and how Much Water to Apply*, University of California Irrigation Program.

Harding, K. J., and P. K. Snyder (2012), Modeling the Atmospheric Response to Irrigation in the Great Plains. Part II: The Precipitation of Irrigated Water and Changes in Precipitation Recycling, *J. Hydrometeor*, *13*(6), 1687–1703, doi:10.1175/JHM-D-11-099.1.

Hoerling, M., J. Eischeid, A. Kumar, R. Leung, A. Mariotti, K. Mo, S. Schubert, and R. Seager (2014), Causes and Predictability of the 2012 Great Plains Drought, *Bull. Amer. Meteor. Soc.*, *95*(2), 269–282, doi:10.1175/BAMS-D-13-00055.1.

Hohenegger, C., P. Brockhaus, C. S. Bretherton and C. Schär (2009), The soil moisture-precipitation feedback in simulations with explicit and parameterized convection, *Journal of Climate*, 22(19), pp.5003-5020, doi:

Hoyos, I., F. Dominguez, J. Cañón-Barriga, J. A. Martínez, R. Nieto, L. Gimeno, and P. A. Dirmeyer (2017), Moisture origin and transport processes in Colombia, northern South America, *Climate Dynamics*, *50*(3-4), 971–990, doi:10.1007/s00382-017-3653-6.

Hu, H., and F. Dominguez (2015), Evaluation of oceanic and terrestrial sources of moisture for the North American monsoon using numerical models and precipitation stable isotopes, *J. Hydrometeor*, *16*(1), 19–35, doi:10.1175/JHM-D-14-0073.1.

Huang, X., and P. A. Ullrich (2016), Irrigation impacts on California's climate with the variable-resolution CESM, *Journal of Advances in Modeling Earth Systems*, *8*(3), 1151–1163, doi:10.1002/2016MS000656.

Huber, D., D. Mechem, and N. Brunsell (2014), The Effects of Great Plains Irrigation on the Surface Energy Balance, Regional Circulation, and Precipitation, *Climate 2014, Vol. 2, Pages 103-128*, *2*(2), 103–128, doi:10.3390/cli2020103.

Huffman, G. J., D. T. Bolvin, E. J. Nelkin, D. B. Wolff, R. F. Adler, G. Gu, Y. Hong, K. P. Bowman, and E. F. Stocker (2007), The TRMM Multisatellite Precipitation Analysis (TMPA): Quasi-Global, Multiyear, Combined-Sensor Precipitation Estimates at Fine Scales, *J. Hydrometeor*, *8*(1), 38–55, doi:10.1175/JHM560.1.

Iacono, M. J., J. S. Delamere, E. J. Mlawer, M. W. Shephard, S. A. Clough, and W. D. Collins (2008), Radiative forcing by long-lived greenhouse gases: Calculations with the AER radiative transfer models, *J. Geophys. Res.*, doi:10.1029/2008JD009944.

Kanamaru, H., and M. Kanamitsu (2008), Model Diagnosis of Nighttime Minimum Temperature Warming during Summer due to Irrigation in the California Central Valley, *J. Hydrometeor*, *9*(5), 1061–1072, doi:10.1175/2008JHM967.1.

Kanamitsu, M., and K. C. Mo (2003), Dynamical Effect of Land Surface Processes on Summer Precipitation over the Southwestern United States, *Journal of Climate*, *16*(3), 496–509, doi:10.1175/1520-0442(2003)016<0496:deolsp>2.0.co;2.

Kgatuke, M. M., W. A. Landman, A. Beraki, and M. P. Mbedzi (2008), The internal variability of the RegCM3 over South Africa, *International Journal of Climatology*, 28(4), 505–520, doi:10.1002/joc.1550.

Koster, R. D., and M. J. Suarez (2001), Soil Moisture Memory in Climate Models, *J. Hydrometeor*, *2*(6), 558–570, doi:10.1175/1525-7541(2001)002<0558:smmicm> 2.0.co;2.

Leichter, I. (1974), Moisture flux and precipitation studies of convective storms in western South Dakota using pibal and radar data. Rep. 74-11, Institute of Atmospheric Sciences, South Dakota School of Mines and Technology, 63 pp.

Leng, G., L. R. Leung, and M. Huang (2017), Significant impacts of irrigation water sources and methods on modeling irrigation effects in the ACMELand Model, *Journal of Advances in Modeling Earth Systems*, *9*(3), 1665–1683, doi:10.1002/2016MS000885.

Lo, M.-H., and J. S. Famiglietti (2013), Irrigation in California's Central Valley strengthens the southwestern U.S. water cycle, *Geophys. Res. Lett.*, *40*(2), 301–306, doi:10.1002/grl.50108.

Mahmood, R., S. A. Foster, T. Keeling, K. G. Hubbard, C. Carlson, and R. Leeper (2006), Impacts of irrigation on 20th century temperature in the northern Great Plains, *Global and Planetary Change*, *54*(1-2), 1–18, doi:10.1016/j.gloplacha.2005.10.004.

Marcella, M. P., and E. A. B. Eltahir (2014), Introducing an Irrigation Scheme to a Regional Climate Model: A Case Study over West Africa, J. Climate, 27(15), 5708–5723, doi:10.1175/jcli-d-13-00116.1.

Martinez, J. A., and F. Dominguez (2014), Sources of Atmospheric Moisture for the La Plata River Basin, *Journal of Climate*, *27*(17), 6737–6753, doi:10.1175/JCLI-D-14-00022.1.

Nakanishi, M., and H. Niino (2006), An Improved Mellor–Yamada Level-3 Model: Its Numerical Stability and Application to a Regional Prediction of Advection Fog, *Boundary-Layer Meteorol*, *119*(2), 397–407, doi:10.1007/s10546-005-9030-8.

National Centers for Environmental Prediction/National Weather Service/NOAA/U.S. Department of Commerce (2000), NCEP FNL Operational Model Global Tropospheric Analyses, continuing from July 1999, https://doi.org/10.5065/D6M043C6, Research Data Archive at the National Center for Atmospheric Research, Computational and Information Systems Laboratory, Boulder, Colo.

Nelson, B. R., O. P. Prat, D. J. Seo, and E. Habib (2016), Assessment and Implications of NCEP Stage IV Quantitative Precipitation Estimates for Product Intercomparisons, *Wea. Forecasting*, *31*(2), 371–394, doi:10.1175/WAF-D-14-00112.1.

NOAA National Weather Service (NWS) Radar Operations Center (1991): NOAA Next Generation Radar (NEXRAD) Level 2 Base Data. NOAA National Centers for Environmental Information. doi:10.7289/V5W9574V [accessed in June 2017]

Orth, R., and S. I. Seneviratne (2012), Analysis of soil moisture memory from observations in Europe, *Journal of Geophysical Research: Atmospheres*, *117*(D15), n/a–n/a, doi:10.1029/2011JD017366.

Ozdogan, M., and G. Gutman (2008), A new methodology to map irrigated areas using multi-temporal MODIS and ancillary data: An application example in the continental US, *Remote Sensing of Environment*, *112*(9), 3520–3537, doi:10.1016/j.rse.2008.04.010.

Ozdogan, M., M. Rodell, H. K. Beaudoing, and D. L. Toll (2010), Simulating the Effects of Irrigation over the United States in a Land Surface Model Based on Satellite-Derived Agricultural Data, *J. Hydrometeor*, *11*(1), 171–184, doi:10.1175/2009JHM1116.1.

Pei, L., N. Moore, S. Zhong, A. D. Kendall, Z. Gao, and D. W. Hyndman (2016), Effects of irrigation on summer precipitation over the United States, *Journal of Climate*, *29*(10), 3541–3558, doi:10.1175/JCLI-D-15-0337.1.

Pielke, R. A. (2001), Influence of the spatial distribution of vegetation and soils on the prediction of cumulus Convective rainfall, *Reviews of Geophysics*, *39*(2), 151–177, doi:10.1029/1999RG000072.

Puma, M. J., and B. I. Cook (2010), Effects of irrigation on global climate during the 20th century, *J. Geophys. Res.*, *115*(D16), D16120–15, doi:10.1029/2010JD014122.

Qian, Y., M. Huang, B. Yang, and L. K. Berg (2013), A Modeling Study of Irrigation Effects on Surface Fluxes and Land–Air–Cloud Interactions in the Southern Great Plains, *J. Hydrometeor*, *14*(3), 700–721, doi:10.1175/JHM-D-12-0134.1.

Sacks, W. J., B. I. Cook, N. Buenning, S. Levis, and J. H. Helkowski (2009), Effects of global irrigation on the near-surface climate, *Climate Dynamics*, *33*(2-3), 159–175, doi:10.1007/s00382-008-0445-z.

Saeed, F., S. Hagemann, S. Saeed and D. Jacob (2013), Influence of mid-latitude circulation on upper Indus basin precipitation: the explicit role of irrigation. *Climate Dynamics.* Vol. 40, Issue 1-2, pp. 430-440. DOI: 10.1007/s00382-012-1480-3

Seneviratne, S. I. et al. (2006), Soil moisture memory in AGCM simulations: Analysis of global land-atmosphere coupling experiment (GLACE) data, *J. Hydrometeor*, *7*(5), 1090–1112, doi:10.1175/JHM533.1.

Seo, D. J., and J. P. Breidenbach (2002), Real-time correction of spatially nonuniform bias in radar rainfall data using rain gauge measurements, *J. Hydrometeor*, *3*(2), 93–111, doi:10.1175/1525-7541(2002)003<0093:RTCOSN>2.0.CO;2.

Schmitz, J. T., and S. L. Mullen (1996), Water Vapor Transport Associated with the Summertime North American Monsoon as Depicted by ECMWF Analyses, *Journal of Climate*, *9*(7), 1621–1634, doi:10.1175/1520-0442(1996)009<1621:wvtawt>2.0.co;2.

Siebert, S., V. Henrich, K. Frenken, and J. Burke (2013), Global Map of Irrigation Areas Version 5, B. Rheinische Friedrich-Wilhelms-Univ., Germany/Food and Agric. Organ. of the U. N., Rome.

Skamarock, W. C., J. B. Klemp, J. Dudhia, D. O. Gill, D. M. Barker, M. G. Duba, X.-Y. Huang, W. Wang, and J. G. Powers (2008), *A description of the advanced research WRF version 3, NCAR Technical Note*.

Sorooshian, S., J. Li, K. L. Hsu, and X. Gao (2011), How significant is the impact of irrigation on the local hydroclimate in California's Central Valley? Comparison of model results with ground and remote-sensing data, *Journal of Geophysical Research: Atmospheres*, *116*(D6), D06102, doi:10.1029/2010JD014775.

Tang, Q., and S. Xie (2015), The ARM Best Estimate Station-based Surface (ARMBESTNS) Data set. United States: N. p., Web. doi:10.5439/1178332.

Tang, Q., S. Xie, Y. Zhang, T. J. Phillips, J. A. Santanello, D. R. Cook, L. D. Riihimaki, and K. L. Gaustad (2018), Heterogeneity in Warm-Season Land-Atmosphere Coupling Over the U.S. Southern Great Plains, J. Geophys. Res., 123, 7867–7882, doi:10.1029/2018JD028463.

Taylor, C. M., C. E. Birch, D. J. Parker, N. Dixon, F. Guichard, G. Nikulin, and G. M. S. Lister (2013), Modeling soil moisture‐precipitation feedback in the Sahel: Importance of spatial scale versus convective parameterization, *Geophys. Res. Lett.*, 40(23), 6213–6218, doi:10.1002/2013GL058511.

Thompson, G., P. R. Field, R. M. Rasmussen, and W. D. Hall (2008), Explicit Forecasts of Winter Precipitation Using an Improved Bulk Microphysics Scheme. Part II: Implementation of a New Snow Parameterization, *Monthly Weather Review*, *136*(12), 5095–5115, doi:10.1175/2008MWR2387.1.

Villarini, G., and G. A. Vecchi (2012), Twenty-first-century projections of North Atlantic tropical storms from CMIP5 models, *Nature Climate Change*, 2(8), 604–607, doi:10.1038/nclimate1530.

Wei, J., Q. Jin, Z.-L. Yang, and P. A. Dirmeyer (2016), Role of ocean evaporation in California droughts and floods, *Geophys. Res. Lett.*, *43*(12), 6554–6562, doi:10.1002/2016GL069386.

Yang, B., Y. Qian, G. Lin, R. Leung, and Y. Zhang (2012), Some issues in uncertainty quantification and parameter tuning: a case study of convective parameterization scheme in the WRF regional climate model, *Atmospheric Chemistry and Physics*, *12*(5), 2409–2427, doi:10.5194/acp-12-2409-2012.

Yang, B., Y. Zhang, Y. Qian, J. Tang, and D. Liu (2016), Climatic effects of irrigation over the Huang-Huai-Hai Plain in China simulated by the weather research and forecasting model, *Journal of Geophysical Research: Atmospheres*, *121*(5), 2246–2264, doi:10.1002/2015JD023736.

Yang, Z., F. Dominguez, X. Zeng, H. Hu, H. Gupta, and Ben Yang (2017), Impact of Irrigation over the California Central Valley on Regional Climate, *J. Hydrometeor*, *18*(5), 1341–1357, doi:10.1175/JHM-D-16-0158.1.

Zhang, J. et al. (2016), Multi-Radar Multi-Sensor (MRMS) quantitative precipitation estimation: Initial operating capabilities, *Bull. Amer. Meteor. Soc.*, *97*(4), 621–638, doi:10.1175/BAMS-D-14-00174.1.

Figure Caption List:

Figure 1: Model domain consists of 1404 grid cells in the zonal direction and 810 in the meridional direction. Blue boxes indicate major irrigated regions in the US. Red boxes show the locations of downwind regions. The snippet shows the locations of measurement sites that measure precipitation, temperature and energy fluxes in the southern Great Plains. Red dots (blue circles) indicate site locations where precipitation and air temperature are extracted in 2011 (2012). Red (blue) triangles indicate site locations where surface energy fluxes are extracted in 2011 (2012).

Figure 2: Irrigation rate over each irrigated region shown in Figure 1. Results are for grid cells with irrigation fraction greater than 0.1.

Figure 3: a) - f) Averaged daily precipitation rate (mm day-1) from May to October 2012 for a) TRMM, b) Stage IV, c) NSSL MRMS, d) PRISM, e) WRF CNTL simulation and f) WRF IRRG simulation). g) WRF bias calculated using WRF CNTL minus PRISM. f) WRF bias calculated using WRF IRRG minus PRISM. g) Absolute bias reduction, using absolute value of g) minus absolute value of f) or |CNTL – PRISM| – |IRRG – PRISM|. Positive value indicates less absolute bias and therefore better performance in precipitation in IRRG, and vice versa.

Figure 4: Comparison between WRF and observations at grid cells where observations are available for May through October 2011 and 2012.

Figure 5. Difference in top layer soil moisture (SM diff; 0-10 cm) between the IRRG and CNTL in a) 2011 and b) 2012, averaged over the JJA season. c) and d) similar as a) and b) but for difference in precipitation (PRCP diff). e) and f) similar as a) and b) but for difference in evapotranspiration (ET diff). g) and h) irrigation amount in JJA in 2011 and 2012. Units are in mm day-1.

Figure 6: Changes in each component in the surface water budget at each selected box shown in Figure 1 for JJA in 2011 and 2012.

Figure 7: a) Changes in sensible heat flux induced by irrigation averaged over the two JJAs. b), c) and d) are similar as a) but for latent heat flux, available energy, and surface skin temperature, respectively. The box in (a) indicates the GPs region.

Figure 8: a) Changes in simulated incoming shortwave radiation due to irrigation averaged over the two JJAs. b), c) and d) are similar as a) but for incoming longwave radiation, outgoing longwave radiation and net radiation, respectively. The box in (a) indicates the GPs region.

Figure 9: a) Spatial pattern of changes in atmospheric water storage (dPW) induced by irrigation in 2011 JJA. b) Changes in moisture flux divergence (MFD) induced by irrigation (shading) for 2011 JJA, changes in integrated water vapor flux (IWVF) induced by irrigation (vectors). c) and d) are similar as a) and b) but for 2012 JJA.

Figure 10: Region specific atmospheric water budget components. Blue (red) represents simulation without (with) irrigation.

Figure 11: Line integral of integrated moisture flux across each border of the regions delineated in Figure 1. West and east (south and north) mean the moisture amount that transport into and out of the region in the zonal (meridional) direction. Positive (negative) value indicates moisture into (out of) the box. Net indicates the summation of moisture fluxes from all four borders.

Positive net value indicates net gain of moisture due to horizontal moisture transport and vice versa.

Figure 12: (Left) Fraction of precipitation originated as source region ET for the control simulation for 2012 JJA, with ET sources regions defined in the red boxes. (2nd column) Source region ET induced precipitation, obtained by multiply fraction of precipitation with precipitation over each grid cell for WRF CNTL 2012 JJA. (3rd column) Irrigation ET induced precipitation changes. (4th column) Irrigation ET induced precipitation changes in percentage with respect to precipitation in WRF CNTL for 2012 JJA.

Figure 13: Mean vertical profiles of moist static energy (MSE) for the GPs and SE in 2011 JJA and 2012 JJA. Blue (brown) curves indicate daytime (nighttime). Daytime corresponds to 12 p.m. to 02 p.m. in local time. Nighttime corresponds to 12 a.m. to 02 a.m. in local time.

Figure 14: Schematic representation of precipitation, evaporation and recycling ratios for irrigated and downwind regions. P represents precipitation. ET is evapotranspiration. Qnet is the net moisture import/export due to horizontal moisture transport. R is the local recycling ratio. +/- indicates irrigation induced increase/decrease in a specific variable. Arrows indicate horizontal moisture transport across the four facets, and Qnet is equal to their summation.

Figure 1.

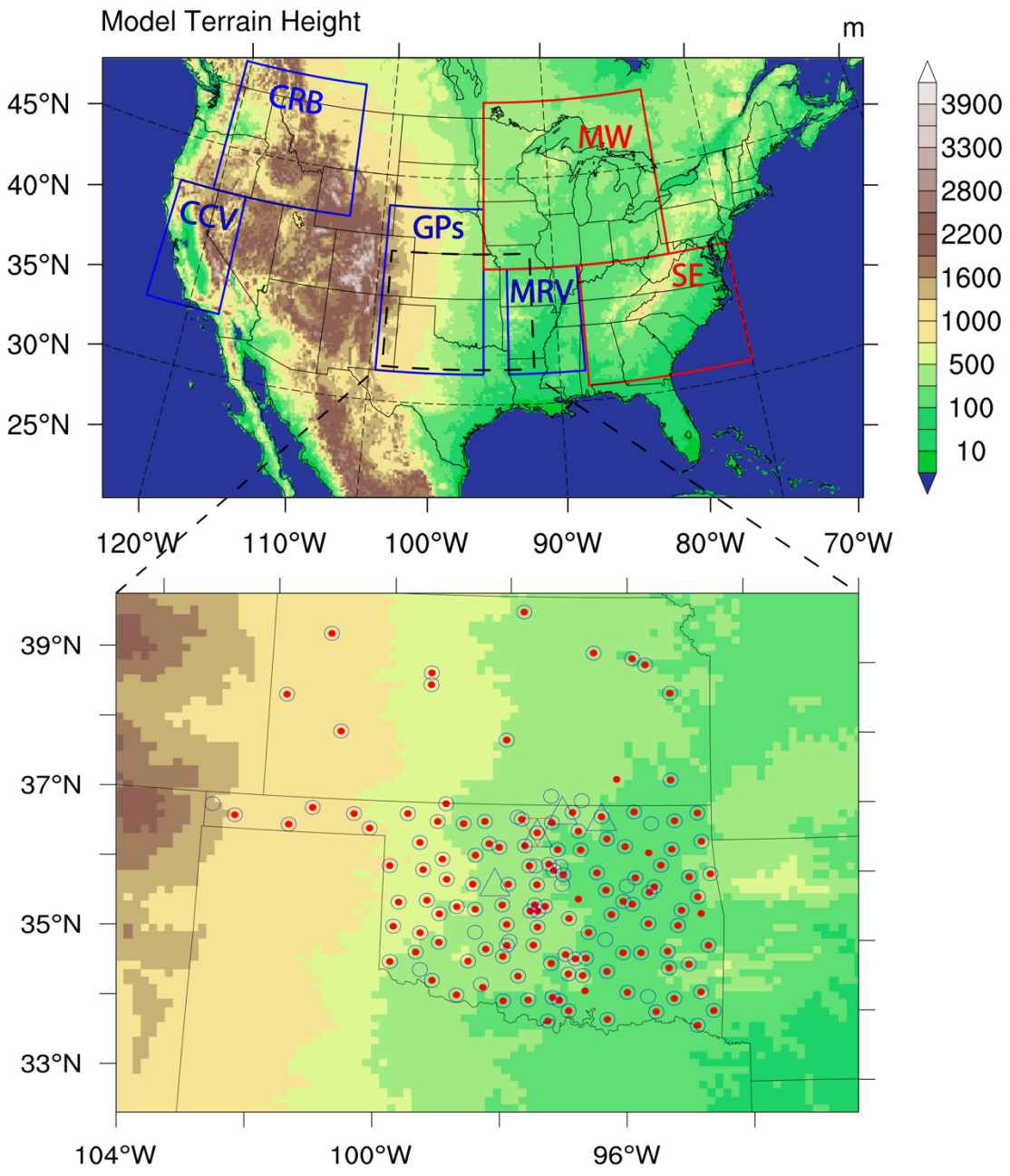
Model Terrain Height
m
CRB
CCV
GPs
MRV
MW
SE
45°N
40°N
35°N
30°N
25°N
120°W
110°W
100°W
90°W
80°W
70°W
3900
3300
2800
2200
1600
1000
500
100
10
39°N
37°N
35°N
33°N
104°W
100°W
96°W

Figure 2.

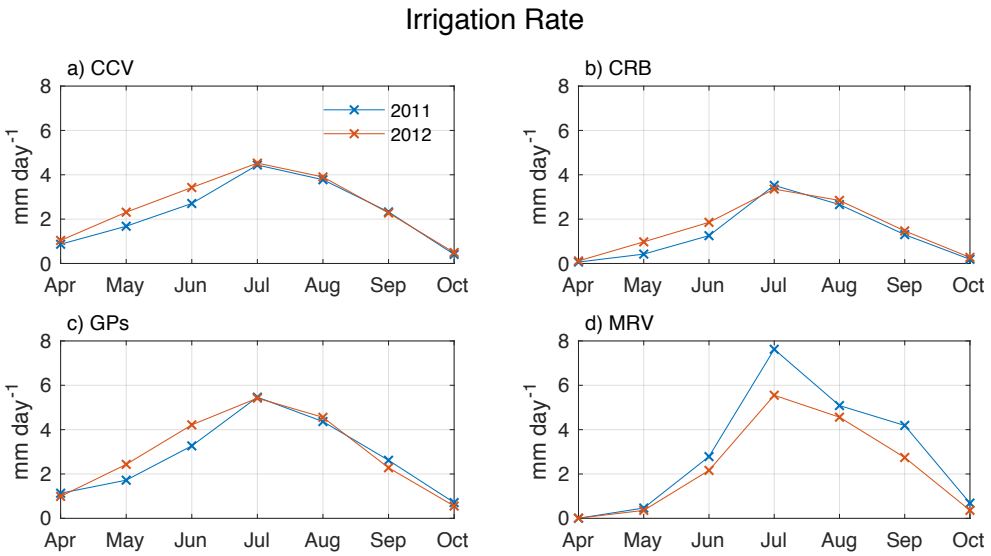
Irrigation Rate
a) CCV
b) CRB
c) GPs
d) MRV
2011
2012
mm day-1
0
2
4
6
8
Apr
May
Jun
Jul
Aug
Sep
Oct

Figure 3.

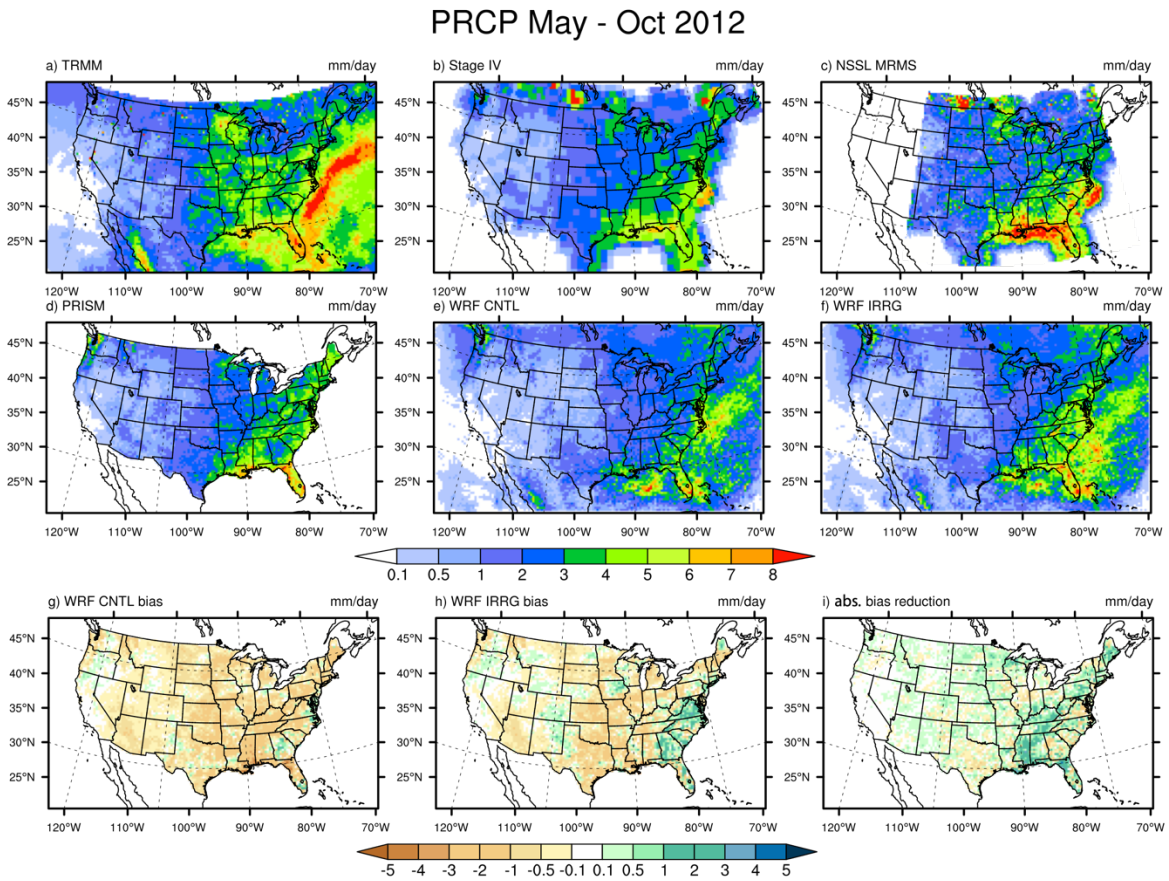
PRCP May - Oct 2012
a) TRMM
b) Stage IV
c) NSSL MRMS
d) PRISM
e) WRF CNTL
f) WRF IRRG
g) WRF CNTL bias
h) WRF IRRG bias
i) abs. bias reduction
mm/day
45°N
40°N
35°N
30°N
25°N
120°W
110°W
100°W
90°W
80°W
70°W
0.1 0.5 1 2 3 4 5 6 7 8
-5 -4 -3 -2 -1 -0.5 -0.1 0.1 0.5 1 2 3 4 5

Figure 4.

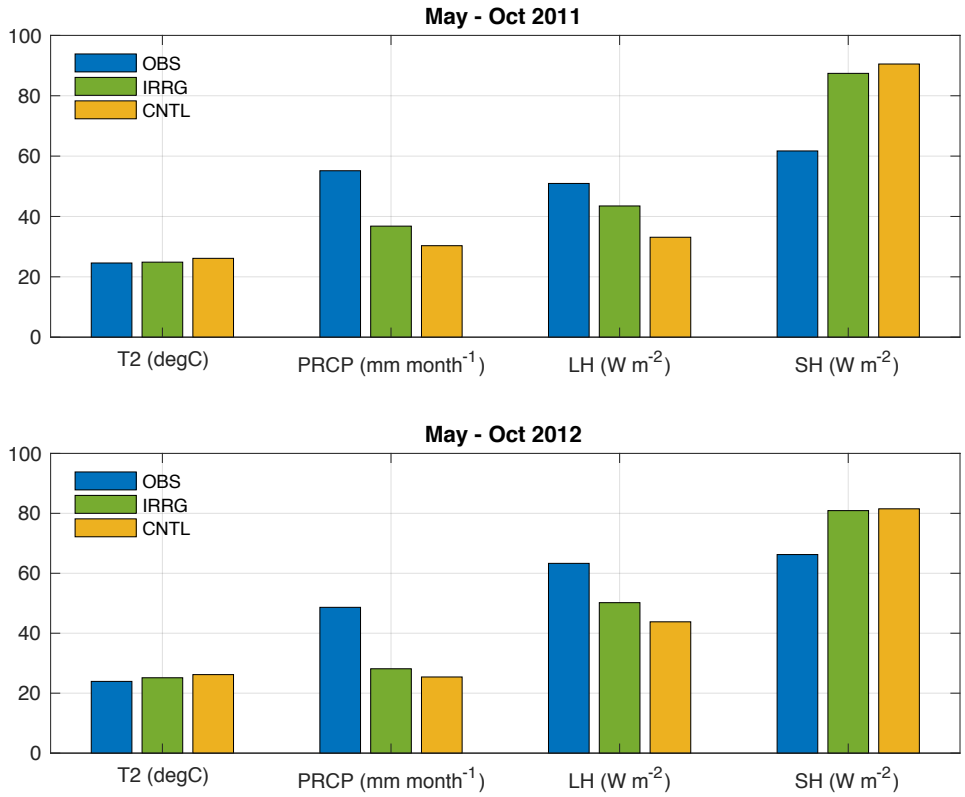
May - Oct 2011
100
80
60
40
20
0
OBS
IRRG
CNTL
T2 (degC)
PRCP (mm month^{-1})
LH (W m^{-2})
SH (W m^{-2})
May - Oct 2012
100
80
60
40
20
0
OBS
IRRG
CNTL
T2 (degC)
PRCP (mm month^{-1})
LH (W m^{-2})
SH (W m^{-2})

Figure 5.

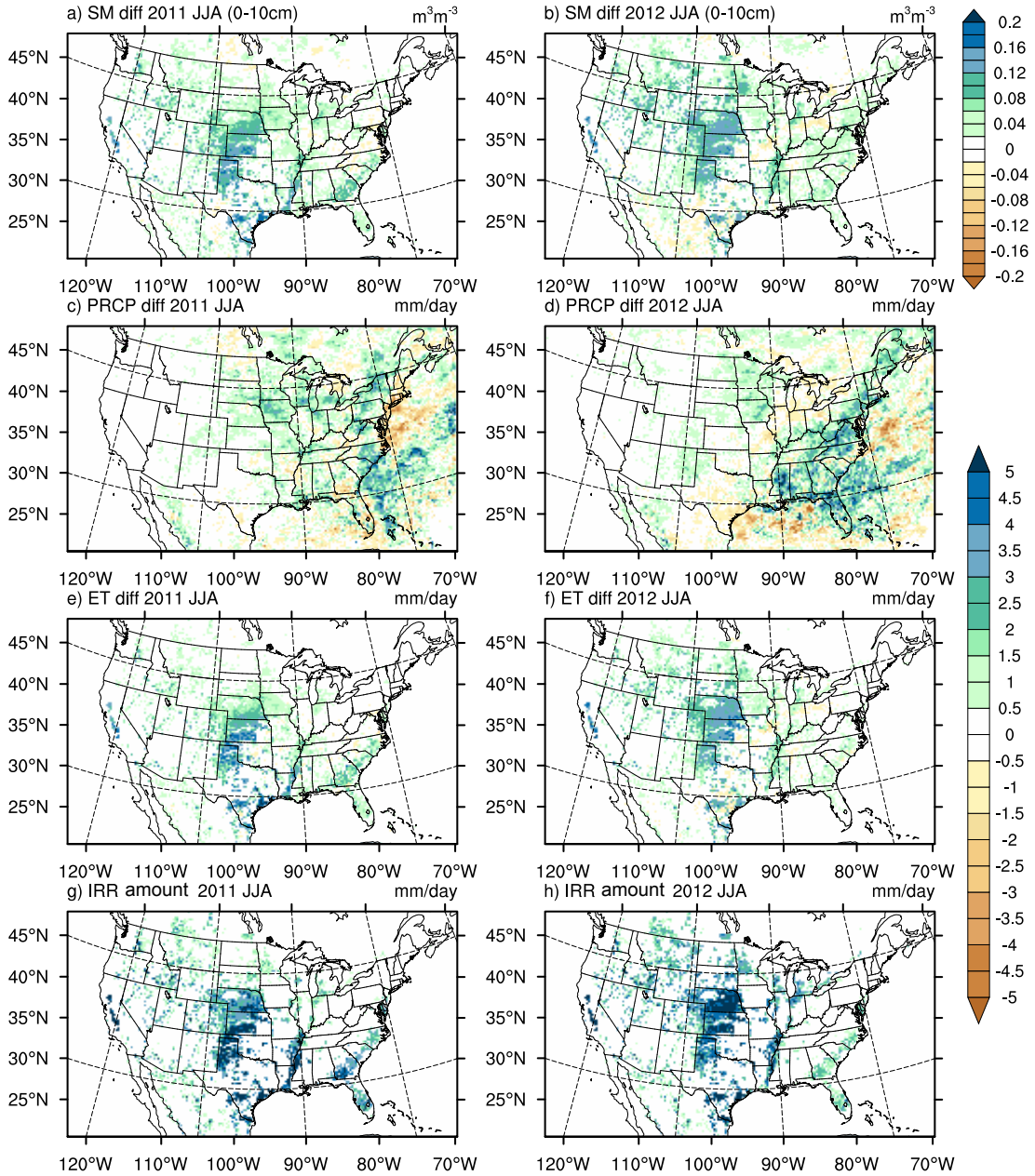
a) SM diff 2011 JJA (0-10cm)
m3m-3
b) SM diff 2012 JJA (0-10cm)
m3m-3
c) PRCP diff 2011 JJA
mm/day
d) PRCP diff 2012 JJA
mm/day
e) ET diff 2011 JJA
mm/day
f) ET diff 2012 JJA
mm/day
g) IRR amount 2011 JJA
mm/day
h) IRR amount 2012 JJA
mm/day
45°N
40°N
35°N
30°N
25°N
120°W
110°W
100°W
90°W
80°W
70°W
0.2
0.16
0.12
0.08
0.04
0
-0.04
-0.08
-0.12
-0.16
-0.2
5
4.5
4
3.5
3
2.5
2
1.5
1
0.5
0
-0.5
-1
-1.5
-2
-2.5
-3
-3.5
-4
-4.5
-5

Figure 6.

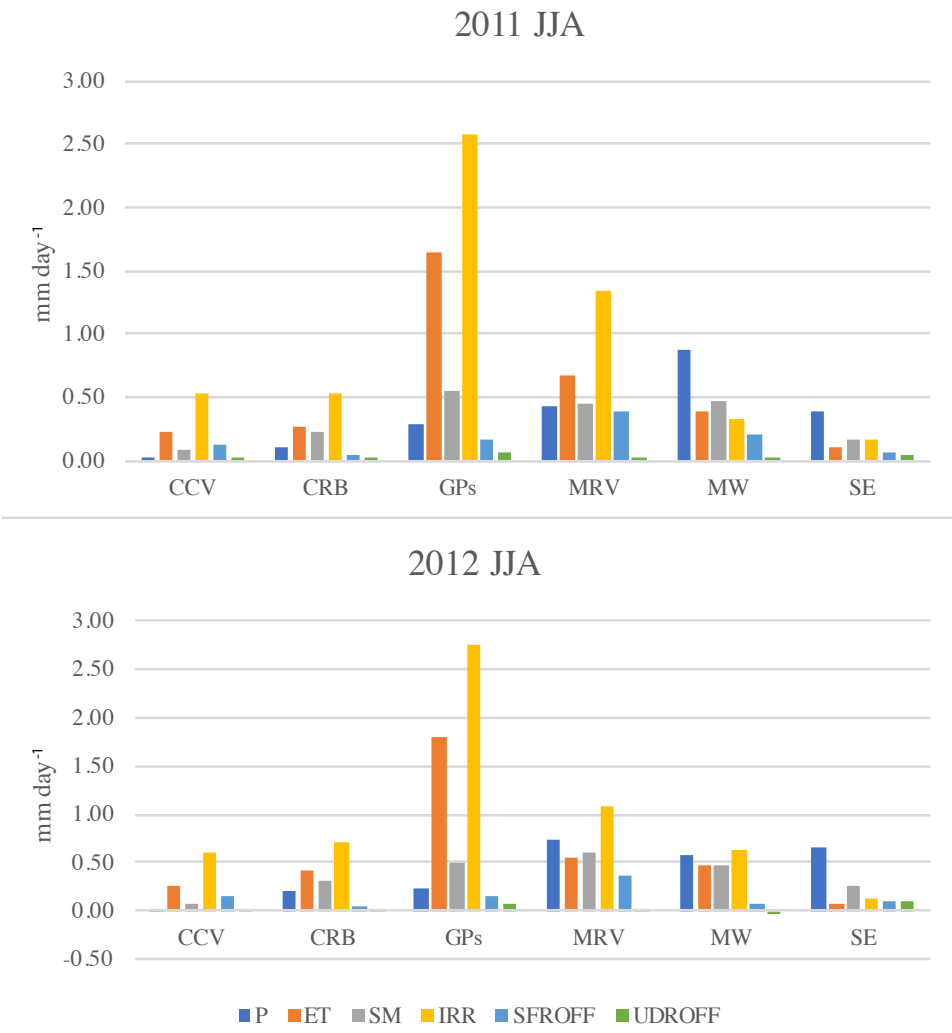
2011 JJA
3.00
2.50
2.00
1.50
1.00
0.50
0.00
mm day-1
CCV
CRB
GPs
MRV
MW
SE
2012 JJA
3.00
2.50
2.00
1.50
1.00
0.50
0.00
-0.50
mm day-1
CCV
CRB
GPs
MRV
MW
SE
P
ET
SM
IRR
SFROFF
UDROFF

Figure 7.

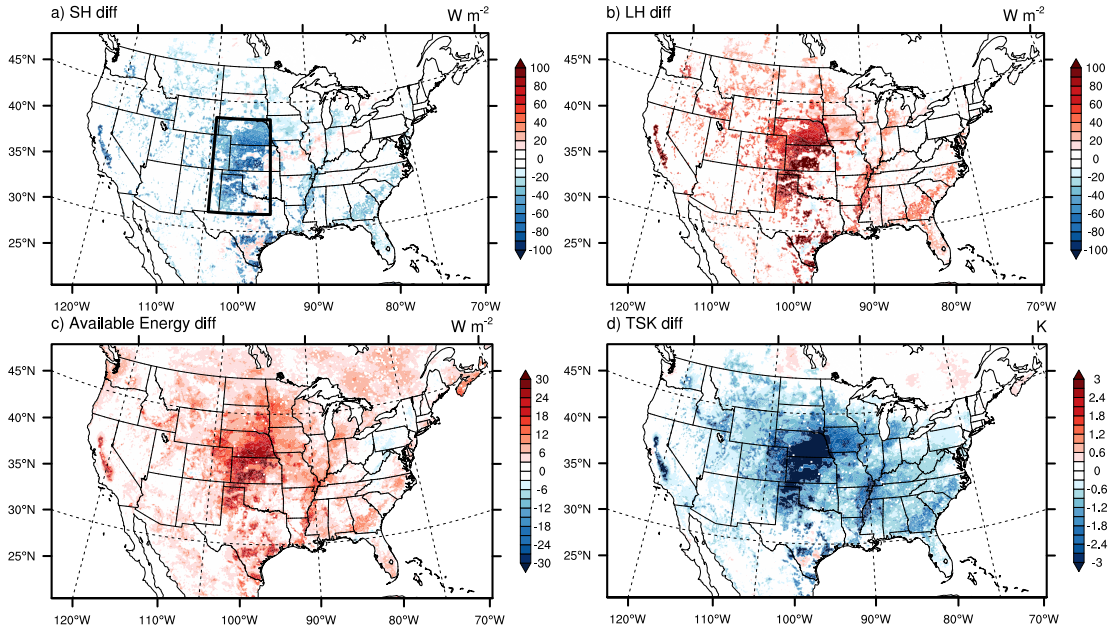
a) SH diff
W m-2
b) LH diff
W m-2
c) Available Energy diff
W m-2
d) TSK diff
K
45°N
40°N
35°N
30°N
25°N
120°W
110°W
100°W
90°W
80°W
70°W
100
80
60
40
20
0
-20
-40
-60
-80
-100
30
24
18
12
6
0
-6
-12
-18
-24
-30
3
2.4
1.8
1.2
0.6
0
-0.6
-1.2
-1.8
-2.4
-3

Figure 8.

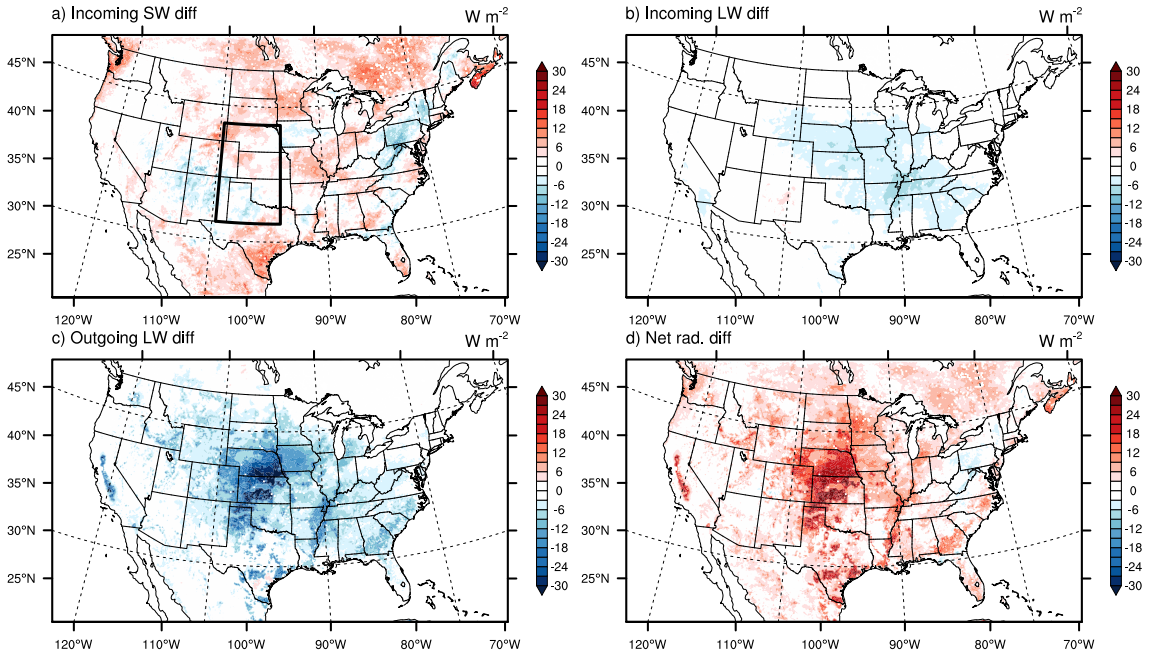
a) Incoming SW diff
b) Incoming LW diff
c) Outgoing LW diff
d) Net rad. diff
W m-2
45°N
40°N
35°N
30°N
25°N
120°W
110°W
100°W
90°W
80°W
70°W
30
24
18
12
6
0
-6
-12
-18
-24
-30

Figure 9.

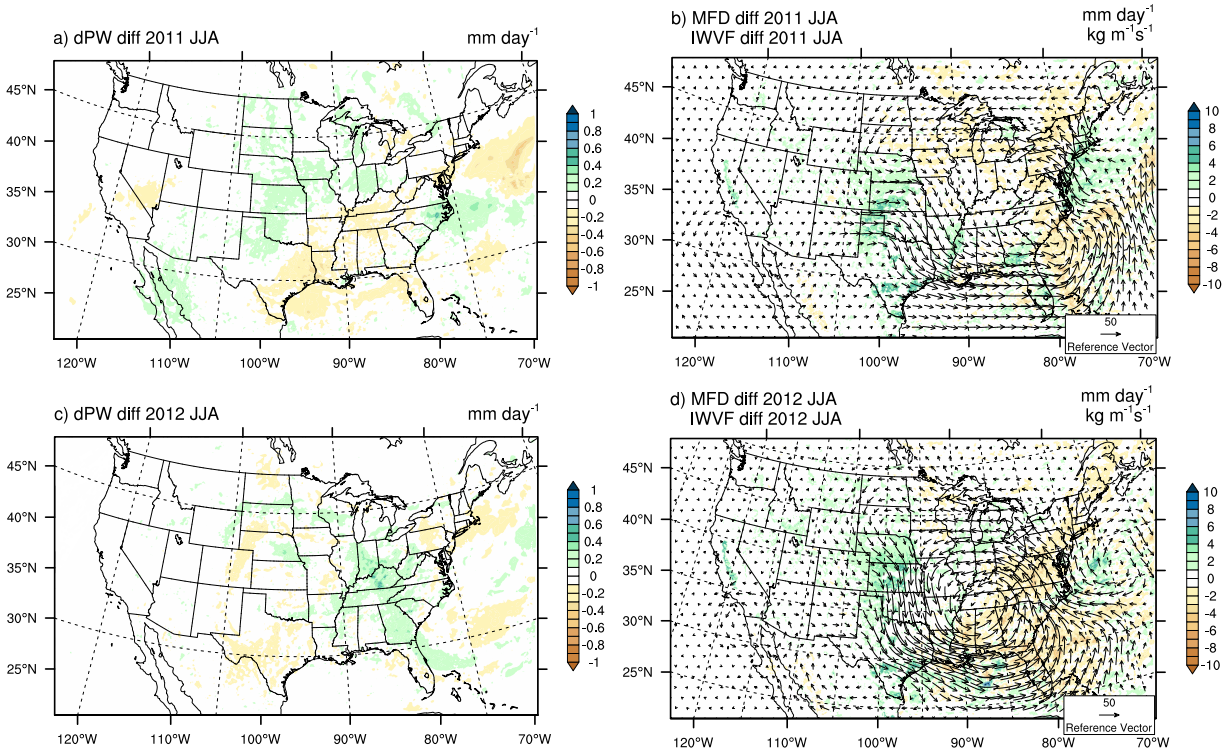
a) dPW diff 2011 JJA
mm day-1
b) MFD diff 2011 JJA
IWVF diff 2011 JJA
mm day-1
kg m-1s-1
c) dPW diff 2012 JJA
mm day-1
d) MFD diff 2012 JJA
IWVF diff 2012 JJA
mm day-1
kg m-1s-1
45°N
40°N
35°N
30°N
25°N
120°W
110°W
100°W
90°W
80°W
70°W
Reference Vector
50

Figure 10.

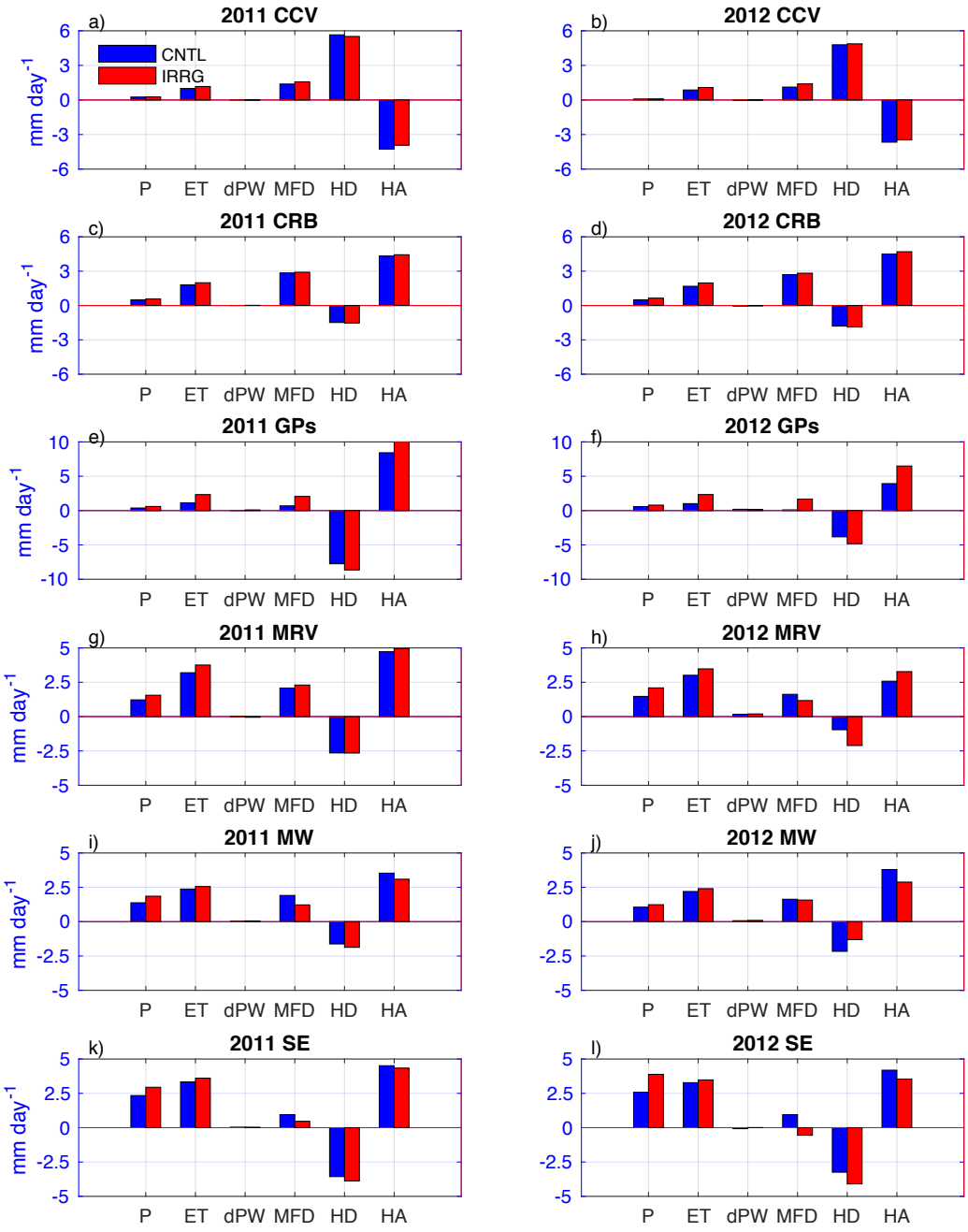
a)
2011 CCV
CNTL
IRRG
b)
2012 CCV
c)
2011 CRB
d)
2012 CRB
e)
2011 GPs
f)
2012 GPs
g)
2011 MRV
h)
2012 MRV
i)
2011 MW
j)
2012 MW
k)
2011 SE
l)
2012 SE
mm day-1
P ET dPW MFD HD HA

Figure 11

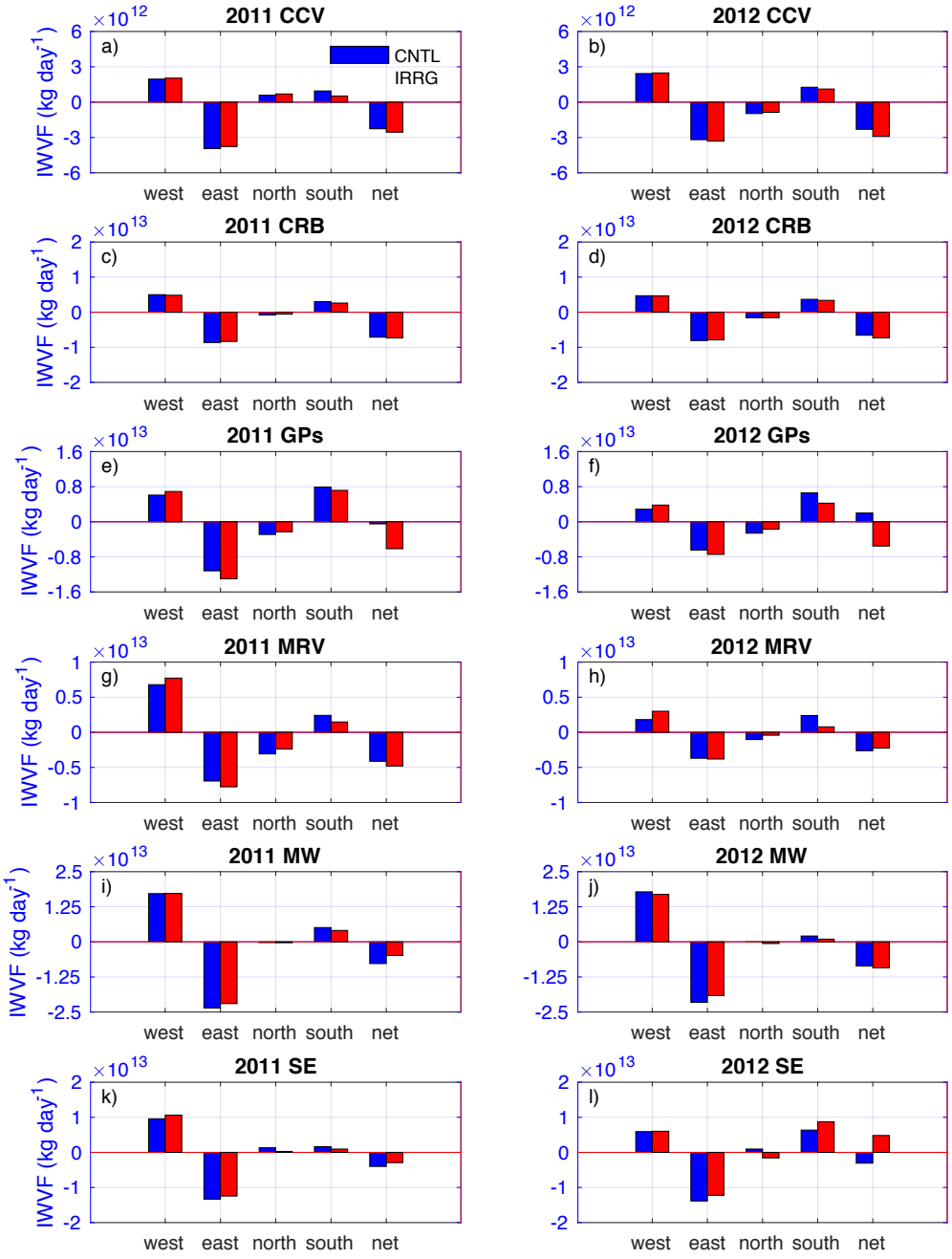
2011 CCV
2012 CCV
2011 CRB
2012 CRB
2011 GPs
2012 GPs
2011 MRV
2012 MRV
2011 MW
2012 MW
2011 SE
2012 SE
a)
b)
c)
d)
e)
f)
g)
h)
i)
j)
k)
l)
CNTL
IRRG
IWVF (kg day-1)
×10^12
×10^13
west
east
north
south
net

Figure 12

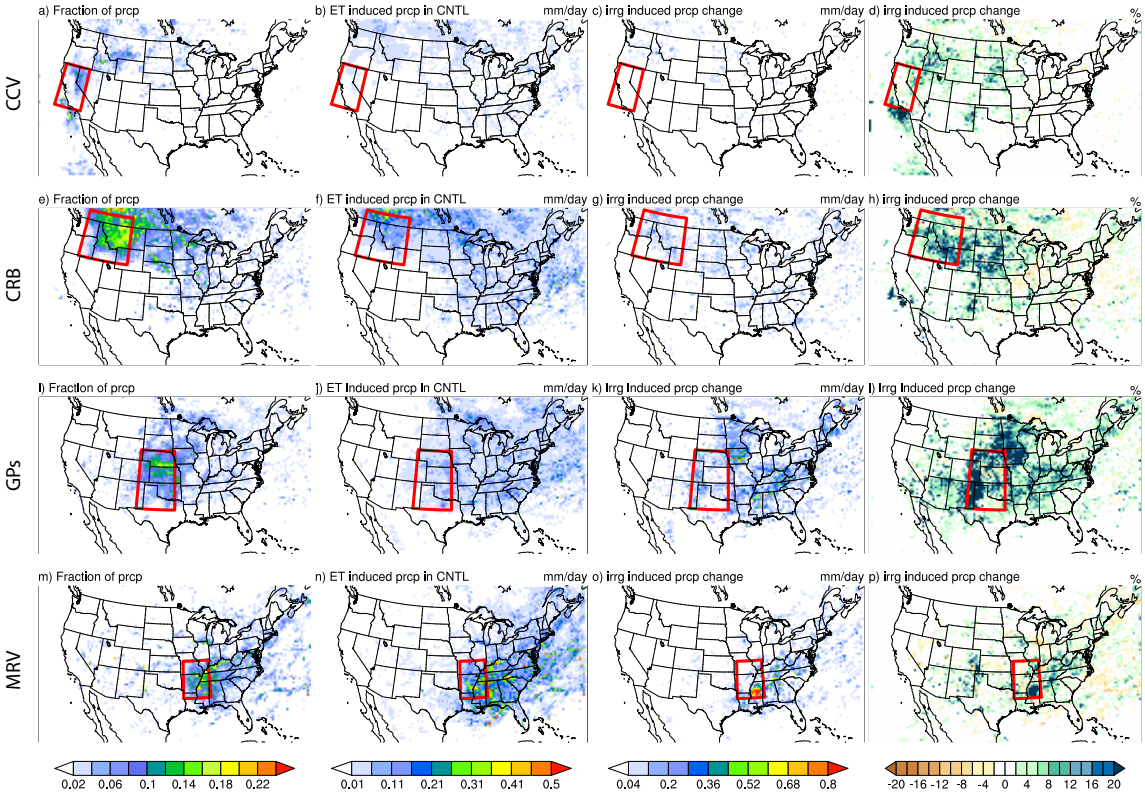
a) Fraction of prcp
b) ET induced prcp in CNTL
mm/day
c) irrg induced prcp change
mm/day
d) irrg induced prcp change
%
CCV
e) Fraction of prcp
f) ET induced prcp in CNTL
mm/day
g) irrg induced prcp change
mm/day
h) irrg induced prcp change
%
CRB
i) Fraction of prcp
j) ET induced prcp in CNTL
mm/day
k) irrg induced prcp change
mm/day
l) irrg induced prcp change
%
GPs
m) Fraction of prcp
n) ET induced prcp in CNTL
mm/day
o) irrg induced prcp change
mm/day
p) irrg induced prcp change
%
MRV
0.02 0.06 0.1 0.14 0.18 0.22
0.01 0.11 0.21 0.31 0.41 0.5
0.04 0.2 0.36 0.52 0.68 0.8
-20 -16 -12 -8 -4 0 4 8 12 16 20

Figure 13

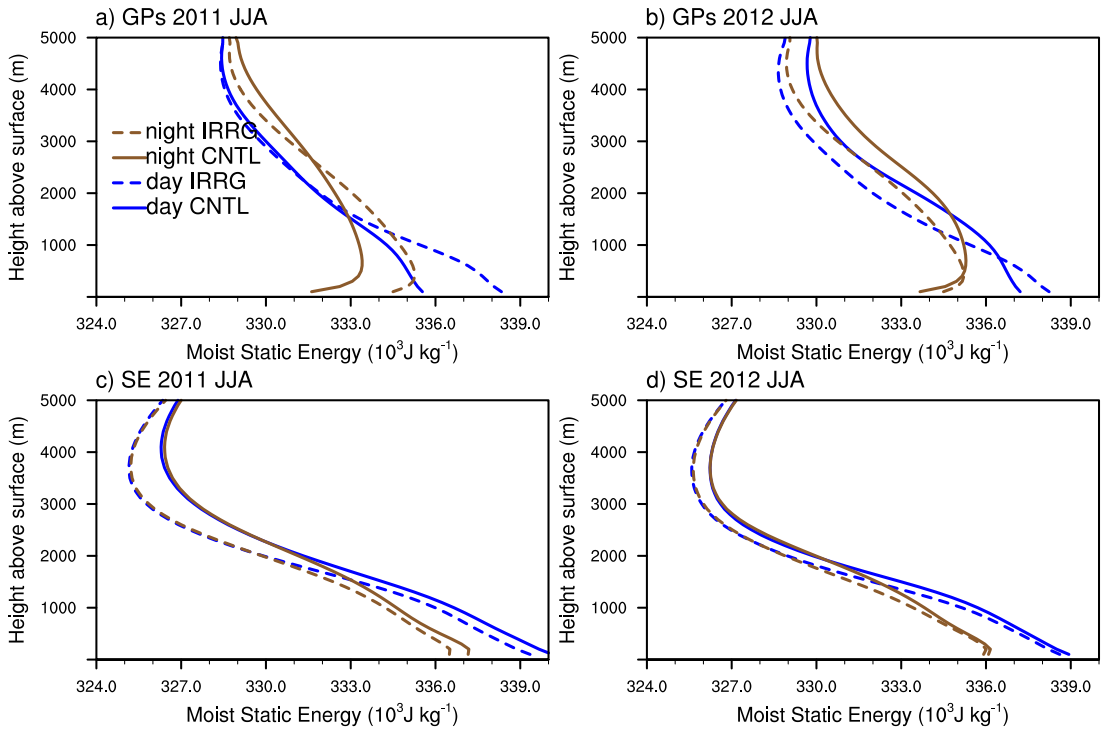
a) GPs 2011 JJA
b) GPs 2012 JJA
c) SE 2011 JJA
d) SE 2012 JJA
night IRRG
night CNTL
day IRRG
day CNTL
Height above surface (m)
Moist Static Energy (10^3J kg^{-1})
5000
4000
3000
2000
1000
324.0
327.0
330.0
333.0
336.0
339.0

Figure 14

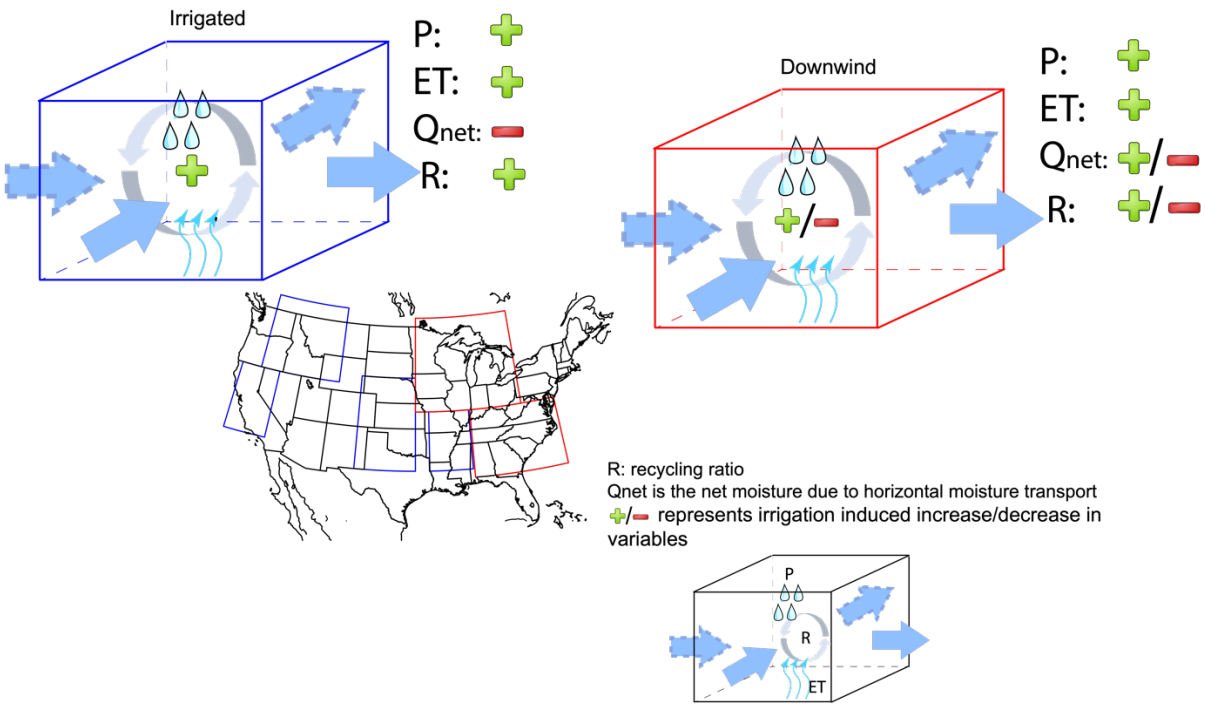
Irrigated
P:
ET:
Qnet:
R:
Downwind
P:
ET:
Qnet:
R:
R: recycling ratio
Qnet is the net moisture due to horizontal moisture transport
+/− represents irrigation induced increase/decrease in variables
P
R
ET